UiT The Arctic University of Norway

Faculty of Science and Technology
Department of Electrical Engineering

Energy Conversion and Control of Hydrogen Fuel Cell Based Electric Transport

Jhalak Nath Subedi

Master thesis [2023]

Abstract

The research investigates the effective utilization of hydrogen fuel cells in electric transport applications, addressing the challenges associated with power generation, energy storage, and control. By implementing the MPPT Perturb and Observe (P&O) technique, the thesis aims to optimize the power output of the fuel cell system, ensuring maximum efficiency and performance. To enhance the overall energy management of the system, a battery and supercapacitor combination is employed as supplementary energy storage. The thesis dives into the design and control strategies required for the seamless integration of these energy conversion systems. The battery's SOC is closely regulated based on the fuel cell voltage, allowing for efficient energy utilization and improved system reliability. The findings of this research contribute to the advancement of hydrogen fuel cell-based electric transport systems. The utilization of MPPT techniques, combined with the integration of battery and supercapacitor systems, offers a promising approach to optimize energy conversion and control. The proposed strategies can lead to enhanced energy efficiency, extended driving range, and improved reliability for future hydrogen fuel cell-based electric transport applications.

Acknowledgements

I would like to extend my heartfelt gratitude to Associate Professor Dr. Bjarte Hoff, my esteemed supervisor, for his exceptional guidance, unwavering support, and invaluable direction throughout the entire process of writing my thesis. His expertise, insightful feedback, and constructive criticism have been instrumental in shaping and refining my research.

I am also deeply indebted to my parents, whose unconditional love, constant encouragement, and unwavering belief in my abilities have been a constant source of inspiration and strength. Their unwavering support has propelled me forward and played a pivotal role in my academic achievements. Additionally, I would like to express my appreciation to all those who have supported and encouraged me along this journey. Your belief in my potential and your words of encouragement have motivated me to overcome challenges and strive for excellence.

I am profoundly grateful to everyone who has contributed to my academic and personal growth. Your support, encouragement, and guidance have been invaluable, and I am forever indebted to each and every one of you.

Thank you all for being an integral part of my journey and for your unwavering support.

Contents

List of Figures

List of Tables

1 Introduction

Non-renewable energy is extremely scarce nowadays, and environmental issues like air pollution from vehicles are a major concern. More people are worried about the development of hybrid electric vehicles ($HEVs$) since conventional fuel vehicles cannot match the current human needs. The depletion of fossil fuel reserves and the escalating difficulties with environmental contamination has made the development of clean energy a hot topic that has an impact on society and the economy [1]. Based on new clean energy without pollution known as proton exchange membrane fuel cell ($PEMFC$), $PEMFC - HEVs$ has great potential for future development. Electric vehicles (EVs) appear to be one of the best answers to the energy crisis and global warming in today's society because they have the advantage of zero fuel consumption and zero emissions [2]. As one example of several sustainable energy technologies, fuel-cell technology offers various benefits like zero emissions, high energy density, safety, and more. Several studies have been conducted recently that use fuel cells for land and water transportation. However, fewer studies have been done on the fuel cell utilized in locomotives than on cars.

In contrast to internal combustion engine vehicles ($ICEVs$), which are responsible for about 28 percent of the world's greenhouse gas (GHG) emissions, electric vehicles (EVs) have grown in popularity due to their sustainable low-carbon features. In-depth research and development of EVs to match the performance of the current $ICEVs$ have been undertaken due to the environmental impact of $ICEVs$ and the depletion of fossil fuels. Changing from $ICEVs$ to EVs can significantly lower GHG emissions over the course of a vehicle's lifetime. To facilitate the phase-out of $ICEVs$ by 2040, several nations, including the UK, France, Norway, China, and Taiwan, have implemented a variety of actions to promote Electric Vehicles [3]. Nevertheless, none of the clean energy alternatives now on the market that is employed in EVs such as fuel cells (FC), supercapacitors, and battery units (BU), can completely replace the $ICEV's$ needs for power, range, and refueling time. Hence, the hybridization of various energy sources and their sizing is a hurdle for Electric Vehicles. As a result, Fuel Cells, Battery Units, and supercapacitors are potential energy sources for hybridization.

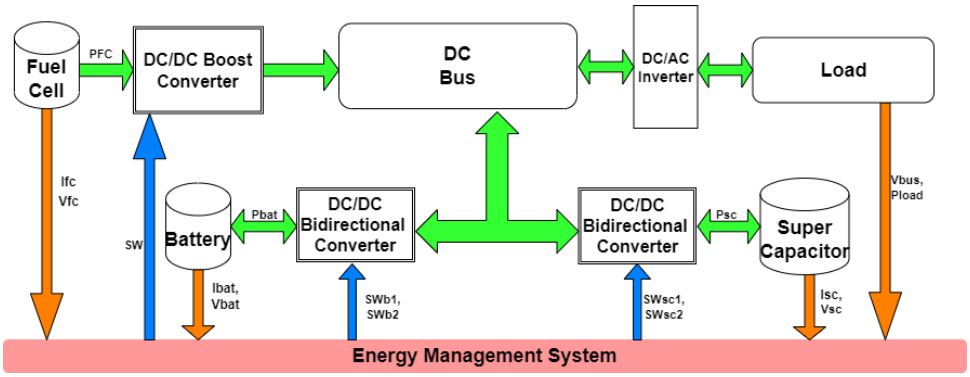

Figure 1.1: Structure Of PEMFC, Battery, SC Hybrid Electric Vehicle.

With Electric Vehicles, three different energy sources are available: batteries, fuel cells, and supercapacitors. The battery is classified as a lithium-ion battery, lead-acid battery, nickel-cadmium battery, or nickel-metal hydride battery. A lead acid battery is currently the most often utilized power source. Lithium, nickel-cadmium, and sodium-sulfur batteries are the main power sources for development. Alkaline, phosphoric acid, molten carbonate, solid oxide, and proton exchange membrane fuel cells are the different types of fuel cells. Nonetheless, *PEM* Fuel Cells are currently used in the majority of automotive applications. This chapter presents an introduction to the concept of a fuel cell hybrid electric vehicle, with a focus on Fuel Cell technology, Battery technology, Fuel Cell system integration, and some insights on different fuel cell and battery powertrain configurations used in the industry.

1.1 Fuel Cell Characteristics

An electrochemical device known as a fuel cell directly transforms the chemical energy of a fuel and an oxidant into electrical energy. A single cell's electrolyte layer is in contact with the porous anode and cathodes on either side, and these three components make up its fundamental physical makeup. In a conventional fuel cell, gaseous fuels are continually delivered into the cathode (positive electrode) compartment, while an oxidant(such as oxygen from the air) is continuously fed into the anode (negative electrode).

Alkaline fuel cells (*AFC*), proton exchange membrane fuel cells (*PEMFC*), phosphoric acid fuel cells (*PAFC*), molten carbonate fuel cells (*MCFC*), and solid-oxide fuel cells (*SOFC*) are only a few examples of the several varieties of fuel cells that exist [4]. The characteristics of each fuel cell vary in a variety of ways, including the types of electrolytes used, the operating temperature range, the peak system efficiency, and the output power level. As a result, different application sectors are suitable for each fuel cell, as shown in Table 1.1.

PEMFCs are particularly well suited for automotive applications due to their advanced features, including their high power density and quick start-up capacity [4]. As a result, whenever the phrase

"fuel cell" is used in this thesis, it specifically refers to PEMFC unless otherwise stated.

Table 1.1: Comparison of different types of fuel cell.

Fuel Cell type	Electrolyte Type	Operation Temperature Range	System Output power Level	System Efficiency	Typical Application Fields
PEMFC	Iconic membrane	[50-80]	1 to 250 KW	50 to 60	Automotive
AFC	KOH, NaoH	[64-200]	300 to 5000W	55 to 65	Aerospace
PAFC	H_3PO_4	[180-250]	100 to 1000KW	35 to 50	Power generation
MCFC	KLiCO_3	[600-700]	10KW to 2MW	40 to 60	Power generation
SOFC	Z_rO_2, Y_2O_3	[750-1000]	<100KW	50	Power generation

Despite having similar parts and features to a standard battery, a fuel cell is different in a number of ways. The chemical reactant stored inside the battery itself controls the amount of energy that is available because the battery is an energy storage device. When the chemical reactants are used up, the battery will stop producing electrical energy (i.e. the battery is discharged). The reactants are continuously supplied from an external source in a secondary battery (fuel cell). On the other hand, a fuel cell is a form of energy conversion that, in theory, has the ability to generate electrical energy as long as fuel and oxidant are supplied to the electrodes. The practical operating life of fuel cells is limited by degradation, typically corrosion, or component failure [5].

1.1.1 PEM Fuel Cell

Polymer Electrolyte Membrane Fuel Cells ($PEMFC$) are well known for being appropriate for automotive applications due to their high power density, solid electrolyte, extended lifespan, and low corrosion. Additionally, they function between 50 and 100°C, which makes operation safer and does away with the requirement for thermal insulation [6].

The chemical energy of the reaction between hydrogen and oxygen is converted to electrical energy by a PEMFC as shown in figure 1.2. The proton exchange membrane is commonly perfluoro sulfonic acid (Nafion), which uses water as the charge carrier for effective proton conductivity [8]. Since it uses platinum-based electrodes, which is an expensive metal, it presents a challenge to function with only pure hydrogen.

At the anode, where the platinum-based catalyst's surface is where protons and electrons are separated, hydrogen fuel is given. While the electrons move through an external circuit, the protons move through the membrane to the cathode side of the cell, producing the electrical output of the cell. Protons and electrons combine with oxygen on the cathode side to form water [7].

The electrochemical reactions in a hydrogen fuel cell as PEMFC governing a single fuel cell are

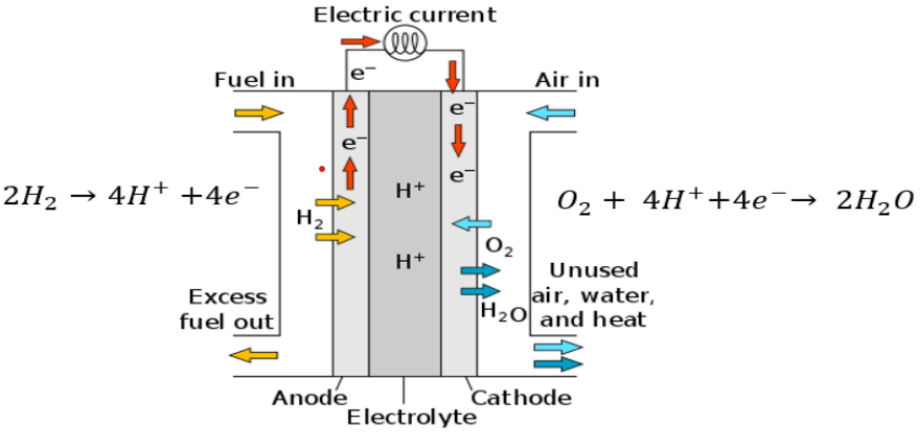

Figure 1.2: Polymer Electrolyte Membrane Fuel Cell (PEMFC) [7].

summarized in eq (1.1-1.3).

$$AnodeReaction : H_2(g) = H^+ + 2e^- \tag{1.1}$$

$$CathodeReaction : \frac{1}{2}O_2 + 2H^+ + 2e^- = H_2O \tag{1.2}$$

The overall reaction of the systen can be written as:

$$H_2(g) + \frac{1}{2}O_2(g) = H_2O + Heat + Electricity \tag{1.3}$$

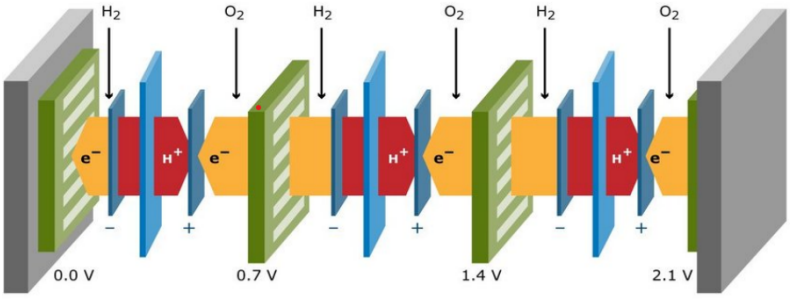

Figure 1.3: PEM Fuel Cell Stack [9].

A single fuel cannot be utilized for the majority of applications since the voltage output ranges from 0.5 V to 1.23 V depending on the ambient conditions. Individual cells are therefore stacked in figure 1.3 to produce a larger voltage and power, precisely like batteries. The term "fuel cell stack" or "stack" is used to describe this collection of cells. The power output from the fuel cell stack is determined by the cell connections and stack size [9].

1.1.2 Fuel Cell System

A fuel cell and its supporting elements together make up the system in Figure 1.4. The cathodic side and the anodic side are the two subsystems that make up the system. The humidifier and compressor on the cathodic side are crucial for controlling the system's cathodic supply. The hydrogen management system, the cooling system, and the water recirculation system make up the anodic side. The system must be run at high pressure, per [10], in order to improve the system's fuel efficiency and power density. Consequently, the compressor is needed to boost the system's air flow rate. A humidifier is used to add moisture to the hot, dry air in order to prevent the membrane from becoming dehydrated. A flow control valve is typically used to supply the hydrogen from the hydrogen storage tanks. The transient responsiveness of the system and its resilience to shifting power needs are controlled by the flow rate of the cathodic air, hydrogen, and recirculating water. Therefore, the key controlling components are the compressor motor, pressure valves, and the water pump or condenser fan speed regulators [11].

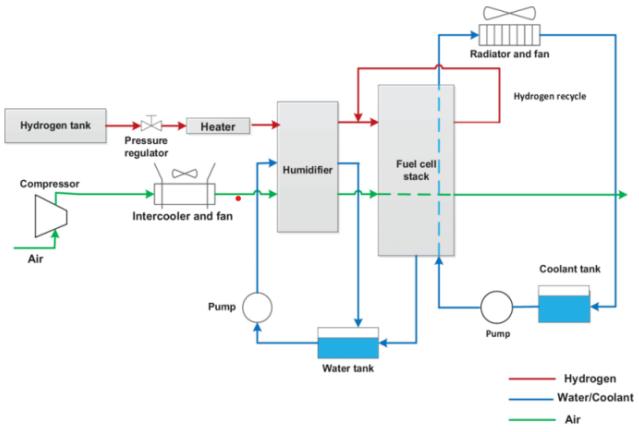

[12]

Figure 1.4: Fuel Cell Schematics [13].

1.2 Powertrain Configurations

In response to the growing problem of increased vehicle emissions, efforts have been ongoing to develop various powertrain configurations. These configurations include battery electric vehicles (BEV), fuel cell electric vehicles ($FCEV$), and fuel cell hybrid electric vehicles ($FCHEV$) [14]. All of these vehicle types operate using an electric motor and incorporate an energy storage system.

1.2.1 Battery Electric Vehicle (BEV)

A BEV is an electric vehicle in which a battery supplies all of the energy. Using a plug-in mechanism, the energy storage device is charged from the grid. In several unique use cases recently, battery-electric trucks have been shown to be competitive enough with their diesel equivalents [15]. This is due to the electrical machine's superior operational efficiency as compared to the traditional internal

combustion engine. Initial and operating costs will significantly decrease with further advancements in battery technology and faster charging methods, paving the way for the widespread adoption of electric commercial vehicles.

1.2.2 Fuel Cell Electric Vehicles (FCEV)

Similar to a car with no exhaust pipe emissions, a fuel cell electric vehicle (*FCEV*) uses solely the fuel cell stack as its energy source. High-pressure hydrogen tanks are used to store the fuel, which is hydrogen. Some vehicles additionally extract the gasoline using a fuel processor on board [14]. In some situations, compared to both traditional diesel trucks and battery-powered trucks, fuel-cell electric trucks are preferred because they can offer a longer range and a higher payload capacity. Additionally, using present technology, charging a battery takes longer than refueling a truck with hydrogen [15].

1.2.3 Fuel Cell Hybrid Electric Vehicles (FCHEV)

Modifying the *FCEV* powertrain results in a new configuration of *FCHEV*, for which both fuel cell battery and supercapacitor function as energy conversion systems, combining the best of all worlds. Depending on the power requirement and drive cycle, ultracapacitors are used in combination with batteries. Figure 1.5 depicts the fuel cell system that combines the battery, supercapacitor energy management unit, fuel cell converter, and inverter. For a specific power demand, the energy management system serves as the foundation for the power split between the battery, supercapacitor, and fuel cell. It is one of the crucial components that determine the system's efficiency. The controller and converter design of the power distribution system for fuel-cell hybrid electric vehicles will be the main emphasis of this thesis.

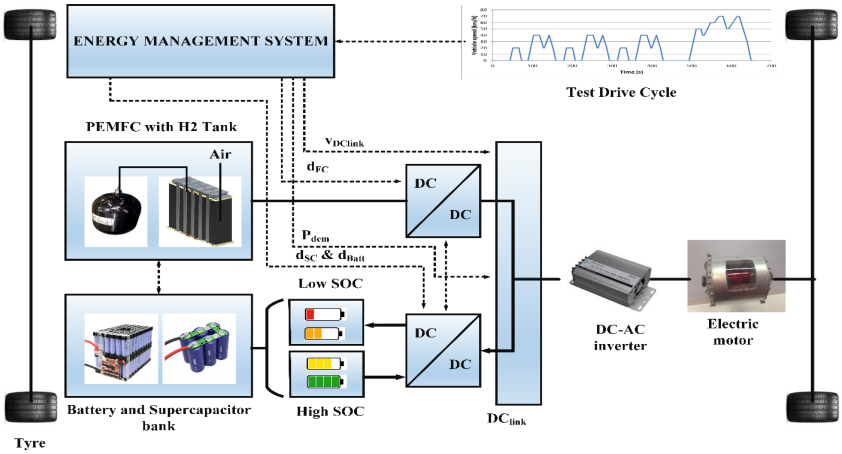

Figure 1.5: Fuel Cell Hybrid Electric Vehicle Energy Mamagement Schematics [16].

1.3 Methodology

This thesis project involves finding the most efficient control method for the energy management system for fuel-cell hybrid electric vehicles. This chapter includes the orientation of the complete project, including the objective, method, and structure of the goal that is fulfilled. It starts with the objective and methods, continues with the formulation of the goal of the thesis, and finally ends with the structure of the thesis that contributes to the energy management strategies used for fuel-cell hybrid electric vehicles.

1.3.1 Objective

The main objective of this thesis is to design and implement a hybrid energy system consisting of a fuel cell, battery, and supercapacitor in a miniature electric vehicle. This thesis features establishing the DC/DC converter control topologies for energy management between the fuel cell, battery, and supercapacitor that meet the requirements of a fuel cell and generate a DC voltage link from a fuel cell. The Super-capacitor and battery unit modules are connected to the DC link with bidirectional buck-boost converters, which ensure the charge and discharge of the battery. The fuel cell module is also connected to the DC link with boost converters, which ensure the boost voltage from the fuel cell. A DC motor, which is controlled via a DC/DC converter, is considered a load. The controller needs to be presented and applied to the converter to have a constant DC voltage link regardless of the ripple in fuel cell current and voltage. Hence, the following objectives were set for the master's thesis:

1. Investigating the operation and feasibility of the selected converter, and designed controller based on the assumptions and requirements.

2. Modelling and simulating the complete system in MATLAB Simulink (R2023a) under various conditions.

3. Studying the performance of the Simulated model and analyzing.

1.3.2 Method

The first part of the thesis is the theory and literature study of the fuel cell and fuel cell-implemented hybrid electric vehicles.

The second part is to implement the preliminary steps required to build the fuel cell in MATLAB or Simulink with the given instructions and data. Simulation on MATLAB is done to check the designed fuel cell result and observe the output of the fuel cell as DC electric current.

The third part of the thesis is the study of the various types of converters that can be implemented in fuel-cell hybrid electric vehicles, the selection of the most efficient converter, the design of the converter, and the observation of the behavior of the fuel-cell hybrid electric vehicle under various changes in fuel and air pressure in the hydrogen PEM fuel cell. The functionality of the auxiliary

elements inside the converter circuit is explained, and mode by mode, the operation of the selected converter is explained.

1.3.3 Structure

Chapter 2 : In the first part, the basic operation of the hydrogen fuel cell is described, which includes a calculation for the cell voltage losses, the double-layer charging effect, the dynamic response, and the thermodynamic response. Secondly, theory and other preliminaries from the specialization project relevant to the thesis are summarized as well. This includes the design of chosen converters, and the design of the controller, for the efficient operation of the hybrid transport system is explained. Furthermore, the investigation or research on the provided fuel cell has been carried out and the result from the investigation is presented and briefly explained.

Chapter 3 In This chapter the simulation of a proton exchange membrane fuel cell ($PEMFC$) and the mathematical model are presented. Also, the simulation of the designed three converters one boost converter for fuel cell and two bidirectional buck-boost converters for battery and supercapacitor are presented. The energy management system or controller is implemented in the various converters and the performance of the system is analyzed in MATLAB Simulink (R2023a).

Chapter 4 This chapter presents an overview of the implemented controller techniques and the control strategy employed in the system. Initially, the explanation of the control strategy applied to the fuel cell battery system is explained. Subsequently, the control strategy employed for the fuel cell, battery, and supercapacitor system is described.

Chapter 5 In this chapter, the outcomes and findings of the converter and controller techniques are thoroughly discussed and analyzed.

Chapter 6 This chapter focuses on discussing the final results obtained from the implemented converters and controller techniques. It includes suggestions for improvements, considerations, and recommendations for future research based on the findings.

Chapter 7 This chapter is the conclusion and gives an overview of the thesis.

2

Fuel Cell Modeling and Converter topologies Operation and Design

This section presents an electrochemical model that can be used to predict the dynamic behavior of fuel cell stacks. firstly mathematical model used to design and simulate fuel cell stack is briefly presented, then, a variety of topologies is presented about $DC-DC$ converters, with two main categories used in the hybrid electric vehicle utilizing hydrogen fuel cell, Single Ended Primary Inductor Type ($SEPIC$) Converter and Conventional Non-Isolated Buck-Boost Bidirectional Converter. Furthermore, the operation of the selected converter is discussed and analyzed.

2.1 PEM fuel Cell Modeling

An electrochemical model that can be used to predict the dynamic behavior of fuel cell stacks with polymer electrolyte membranes is presented in this section. For the best simulation outcomes, this mathematical model uses a set of parameters whose definition is essential. The output voltage of the fuel cell can be presented in terms of its losses as follows:

$$V_{fc} = E_{nernst} - V_{act} - V_{ohm} - V_{con} \tag{2.1}$$

Where $E_{Nernest}$ is the thermodynamic potential of each unit cell and represents its reversible voltage, V_{act} is the activation voltage drop associated with the anode and cathode, V_{ohm} is the ohmic voltage drop associated with the conduction of protons and electrons, and V_{con} is the concentration voltage drop resulting from the decrease in the concentration of oxygen and hydrogen. The first term in 2.1 represents the fuel cell open circuit voltage, while the last three-term represents the loss in this voltage, which can be presented as follows.

2.1.1 Steady State Model

The cell voltage of a *PEM* fuel cell can be represented by a polarization curve. figure 2.1 shows the response of a single cell against varying current densities. The fuel cell's optimal voltage is shown by the horizontal line at the top. When the fuel cell's outer circuit is open, or when no current is flowing across it, the optimum voltage is reached. The ideal fuel cell voltage can be represented by Nernst Equation as:

$$E = E^o - \frac{RT}{2F} ln(PH_2 * PO_2^{(0.5)}) \tag{2.2}$$

Where E^o is the *EMF* at standard pressure and is also called the ideal cell voltage. E is the potential at the thermodynamic equilibrium. R is the universal gas constant, 8.314 $J.mol^-1.K^-1$ and F is the faradays constant, 96,485 are constants, whereas 2 represents the number of electrons passing through the outer circuit. The temperature is denoted by T in kelvin. PH_2) and PO_2 are the partial pressures of the hydrogen and oxygen at the anode and cathode respectively.

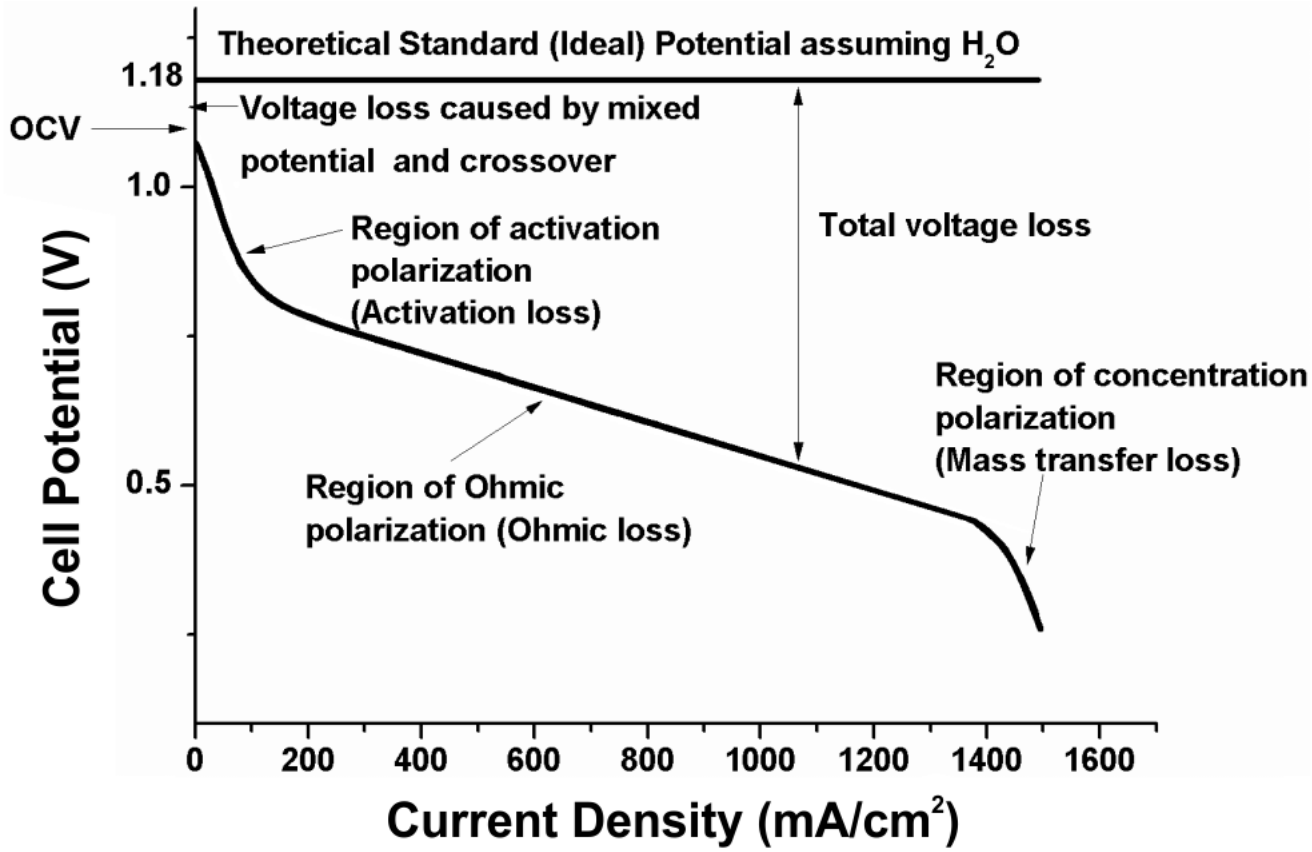

Figure 2.1: Polarization curve of PEMFC .

The equation of cell ideal voltage can be summarized by substituting all the constants:

$$E = 1.229 - 8.5e^-4(T_{cell} - 298.5) + 4.308e^-5[ln(PH_2) + 0.5ln(PO_2)] \tag{2.3}$$

Partial pressures can be represented as :

$$PH_2 = 0.5PH_2o^{sat}[exp(-\frac{1.635J}{T_{cell}^{1.334}}(\frac{P_a}{PH_2o^{sat}}) - 1] \tag{2.4}$$

$$PO_2 = PH_2o^{sat}[exp(-\frac{4.192J}{T_{cell}^{1.334}}(\frac{P_c}{PH_2o^{sat}}) - 1] \tag{2.5}$$

Where:

- P_a=Partial pressure at anode;
- j=current density;
- P_c=Partial pressure at cathode;
- PH_2o^{sat}=saturation pressure of water.

$$log_{10}PH_2o^{sat} = -2.18 + 2.95e^{-2}T_c - 9.18e^{-5}T_c^2 + 1.44e^{-7}T_c^3 \tag{2.6}$$

$$T_C = T_{cell} - 273.15 \tag{2.7}$$

The final voltage produced by the fuel cell is the sum of the ideal voltage and some polarization losses, such as activation loss V_{act}, Ohmic loss V_{ohm}, and Concentration loss V_{con}. According to Figure 2.2, these losses occur at three separate times. Below is a detailed discussion of these losses.

2.1.2 Activation Losses

A fuel cell experiences activation losses in the initial stages of chemical reactions that are going through oxidation and reduction. The slow rate of reaction at the electrodes causes the losses to increase. The fuel cell uses a portion of the total voltage it generates to power the chemical reaction that is occurring. Significant activation losses occur in low-temperature fuel cells and are typically caused by the cathode. The significance of the activation losses decreases with rising temperature. The Tafel equations and the Butler-Völlmer equation are frequently used to model activation losses [[17], [18]]. The simplified equation is:

$$V_{act} = \zeta_1 + \zeta_2 T + \zeta_3 ln(CO_2) + \zeta_4 ln(IFc) \tag{2.8}$$

Where ζ_1, ζ_2,ζ_3,ζ_4 are parametric coefficients taken from [19]. CO_2 represents the concentration of oxygen, which can be calculated from the following equation.

$$CO_2 = \frac{PO_2}{5.08 * 10^6 * e^{-\frac{498}{T_{cell}}}} \tag{2.9}$$

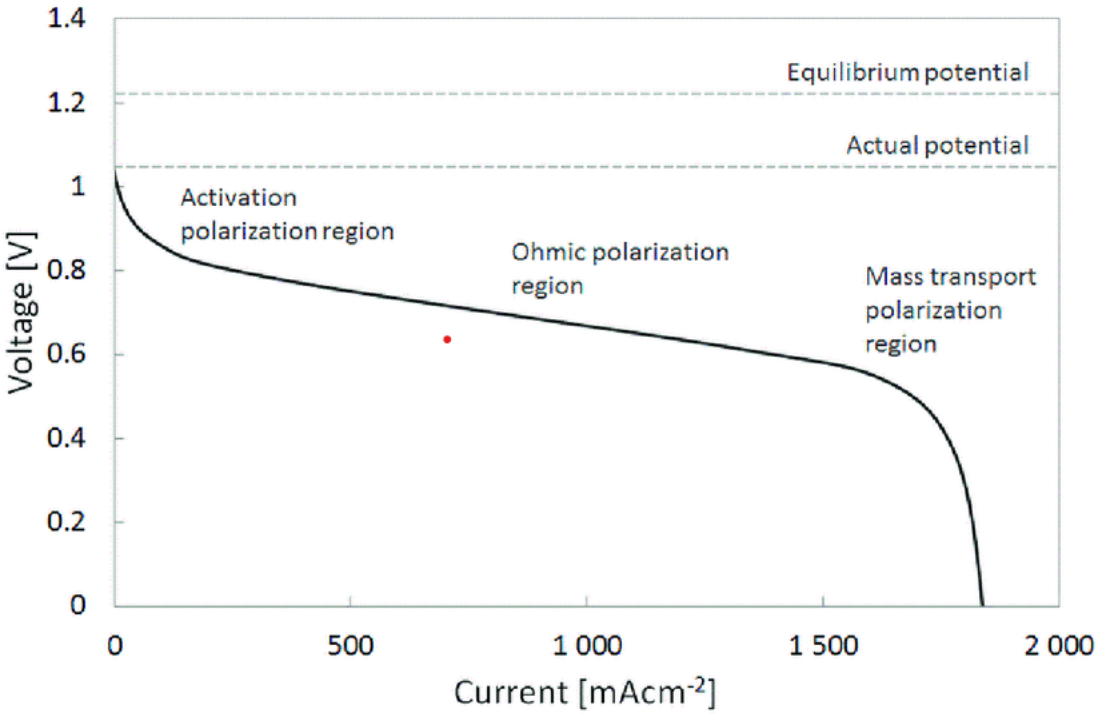

Figure 2.2: Three stages of Voltage losses.

2.1.3 Ohmic Losses

The ohmic losses take place during the second stage, as shown in Figure 2.2. These losses are shown by the stage 2 linear line. Two resistances that occur in the fuel cell are the cause of these losses. First, the electrons encounter resistance as they move through the outside circuit. The protons encounter resistance as they pass through the proton exchange membrane, which is the second factor. The fuel cell's potential is lost as a result of these resistances. Ohm's law can be used to simply explain the voltage drop.

$$V_{ohm} = -Ifc * R_{int} \tag{2.10}$$

Where Ifc is the fuel cell current and R_{int} is the overall internal resistance of the fuel cell. The internal resistance can be represented as a function of temperature and current [17].

$$R_{int} = 1.605 * 10^{-2} - 3.5 * 10^{-5} T_{cell} + 8 * 10^{-5} Ifc \tag{2.11}$$

2.1.4 Concentration Losses

The concentration losses take place in the third and last stages, these losses are also called mass transportation losses. The concentrations of oxygen and hydrogen at the anode and cathode, respectively, are related to these losses. When current densities are higher, these losses are significant. More current is pulled from the $PEMFC$ as the current density rises, increasing the amount of fuel and oxygen consumed. The fuel cell won't function if the current density is raised above the limit, or limiting current density, because there won't be as many reactants because the rate of

consumption will outpace the rate of supply [20].

$$V_{con} = B * ln(1 - \frac{Ifc}{I_{lim}}) \tag{2.12}$$

Where I_{lim} is the limiting current in the fuel cell.

The final output voltage can be calculated by the summation of an ideal voltage and all the voltage drops of the fuel cell.

$$V_{cell} = E - V_{act} - V_{ohm} - V_{con} \tag{2.13}$$

2.1.5 Dynamic and Thermodynamic Losses

Since dynamic activation losses and thermodynamic modeling are also included, the dynamic modeling of a *PEMFC* differs from a steady-state model. Fuel cells respond dynamically mostly because of the charge double layer (CDL). When two different materials come into contact with one another, this phenomenon happens. On the surface, a charge is formed and it is transferred from one material to another. Two more equations need to be modeled in order to examine the dynamic response. The first one is represented by the dynamic activation losses:

$$\frac{dV_{act}}{dt} = \frac{Ifc}{C} - \frac{V_{act}}{R_c C} \tag{2.14}$$

Where R_c is the sum of steady-state activation and concentration losses divided by current, and C is the double-layer capacitance. Equation 2.14 is solved by using a Matlab/Simulink integrator.

$$R_c = \frac{V_{act} + V_{con}}{Ifc} \tag{2.15}$$

The thermodynamic response is given by the second equation. In contrast to a steady-state model, a dynamic model does not assume a constant fuel cell temperature. The fact that all other factors, including the ideal voltage "E," the three voltage drops, and the partial pressures, are calculated using this temperature makes it significant.

$$C_t \frac{dT}{dt} = Ifc(E - V_{cell}) - H(T_{cell} - T_f) \tag{2.16}$$

Where:

- C_t = the total thermal capacitance;
- H = the total heat transfer coefficient;
- T_f = ht reference temperature;
- T_{cell} =the lumped temperature of the fuel cell.

Table 2.1: Parameters of PEM Fuel Cell (H-cell 2.0)

Parameter	Value	unit
$No.ofcells$	14	-
$Activecellarea$	108.8	cm^2
$RatedPower$	30	W
$RatedVoltage$	8.4	V
$RatedCurrent$	3.6	A
$MaxstackTemperature(T)$	55	°C
$Concentrationlosscoefficient$	0.016	V
$Idealgasconstant$	8.31	$J.mol^{-1}.K^{-1}$
$Faradayconstant(F)$	96485.33	c/mol
ζ_1	-0.9514	
ζ_2	$3.12*10^{-3}$	
ζ_3	$7.4*10^{-5}$	
ζ_4	$-1.87*10^{-4}$	
$Limitingcurrent$	25.1	A
$pressureofoxygen$	0.5	atm
$pressureofhydrogen$	1	atm

2.1.6 PEMFC Stack Modeling

A fuel cell consists of various numbers of cells arranged in a manner called a fuel cell stack. The output of the fuel cell can be calculated by taking the product of the number of cells used and the cell output voltage V_{cell}.

$$V_{stack} = n * V_{cell} \tag{2.17}$$

2.1.7 Power of PEM fuel cell

The equation below can be used to calculate the instantaneous electrical power delivered by the cell to the load.

$$P_{fc} = I * V_{fc} \tag{2.18}$$

where V_{fc} is the cell output voltage, and p_{fc} is the output power.

The Simulink model designed for the fuel cell is described in chapter [3].

2.2 Converter Topologies

2.2.1 Single-Ended Primary Inductor Converter (SEPIC)

single-ended primary inductor converter shown in Figure 2.3, is one of the preferred topologies for the Hybrid electric vehicle because of its attractive advantages of having a non-inverted output, by means of coupling energy from the input to the output via a series capacitor. For maximal output voltage during the switching operation, the *SEPIC* converter operates in both buck and boost modes. In order to achieve a challenging output voltage, the ON time will be longer than the OFF time. It is always preferable over buck-boost converters for applications requiring higher power since it may generate non-inverting output, which makes it more noticeable. The limitation is difficult to control its duty cycle and results in poor voltage gain [21] [22].

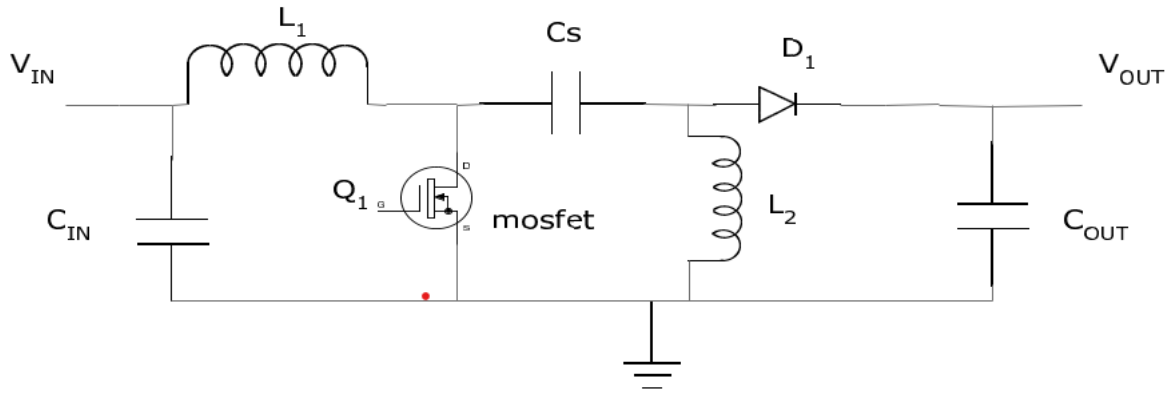

Figure 2.3: Circuit Diagram of SEPIC Converter [22].

Circuit Operation

Continous Conduction mode

If the current flowing through inductor $L1$ never reaches zero, a SEPIC is said to be operating in continuous-conduction mode. The average voltage across capacitor $C_s * (V_{Cs}$ during a $SEPIC's$ steady-state operation is equal to the input voltage (VIN). The only source of load current is provided by the inductor $L2$ because the capacitor C_s serves to block direct current, resulting in a zero average current across it I_{Cs}. Thus, the average current flowing through inductor $L2$ is equal to the average current flowing through the load, making it independent of the input voltage. When average voltages are considered, the following can be written:

$$V_{in} = V_{L1} + V_{Cs} + V_{L2} \tag{2.19}$$

When

$$V_{cs} = V_{in} \tag{2.20}$$

$$V_{L1} = -V_{L2} \tag{2.21}$$

The two inductors can therefore be wound on the same core. The magnitude of the voltages being identical, their mutual inductance effect will be zero. Here, it is assumed that the coil's polarity is accurate. The ripple currents of the two inductors will be identical in size since the voltages are of an equal magnitude. one may sum up the average currents as follows:

$$I_{D1} = I_{L1} - I_{L2} \tag{2.22}$$

Current I_{L1}, and current I_{L2} increases in a negative way, when switch $Q1$ is turned oN. The input source provides the energy needed to increase the current $IL1$. The voltage V_{L2} is approximately $-V_{IN}$ because Q1 is briefly closed, and the instantaneous voltage V_{Cs} is approximately V_{IN}. In order to increase the amount of current in $IL2$ and therefore the energy stored in $L2$, the capacitor Cs provides the energy. The current ICs equals the current $IL1$ when switch $Q1$ is turned off because

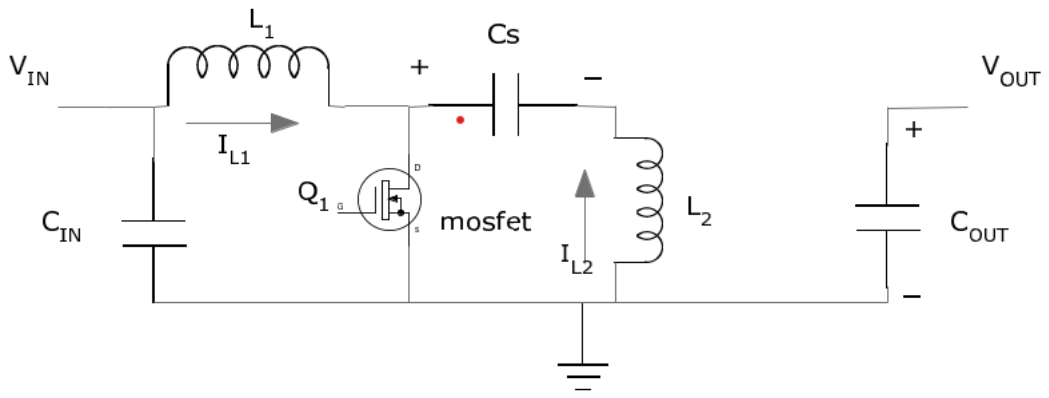

Figure 2.4: SEPIC ON State (Continuous Conduction mode) [22].

the inductors restrict instantaneous changes in current. The current $IL2$ won't change course; in fact, it will continue to move in a negative way. Figure (2.5) shows that a negative $IL2$ will increase the current provided to the load by adding to the current $IL1$. Kirchhoff's current law is used.

$$I_{D1} = I_{Cs} - I_{L2} \tag{2.23}$$

so when Q_1 is off, power is delivered to the load from both L_1 and L_2. Coupling capacitor C_s, is charged by L_1 during the OFF cycle, and recharges L_2 during the ON cycle.

The theoretical waveform of the sepic converter has been shown in Figure 2.6. In [20] explains a novel non-coupled inductor high voltage gain *SEPIC* converter. The converter is simple, and just four additional components are required to modify it. The converter has a number of benefits, including non-inverting output voltage, high efficiency, and high voltage gain. It also has lower voltage stress on the switches. The converter that has been introduced also provides a constant input current, making it appropriate for fuel cell hybrid and renewable energy applications. There are many types of converters proposed to improve the performance of the renewable hybrid electric vehicle such as a high gain bidirectional *SEPIC* converter in [23], a novel switched-coupled inductor

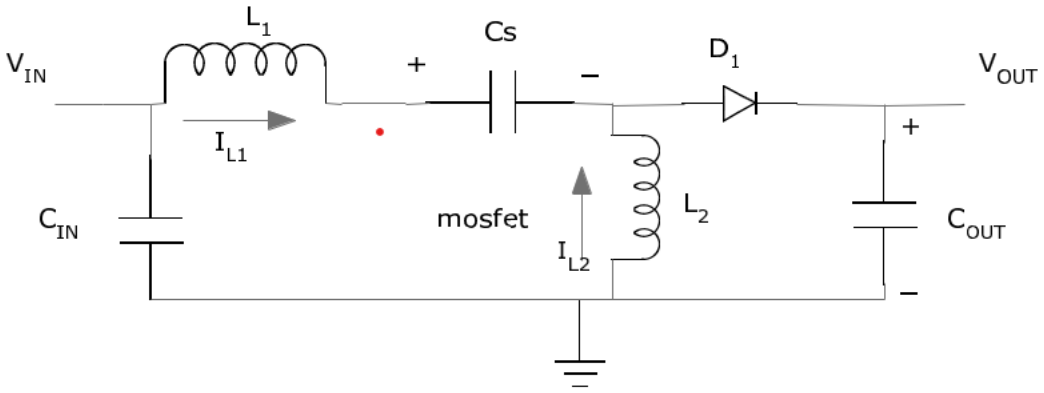

Figure 2.5: SEPIC OFF State (Continuous Conduction mode) [22].

DC – *DC* step-up converter with high conversion ratio is presented in [24], a high step-up *DC* – *DC* converter is discussed in [25], high step-up *Dc* – *Dc* converter with active switched-inductor and passive switched-capacitor network is presented in [26], etc.

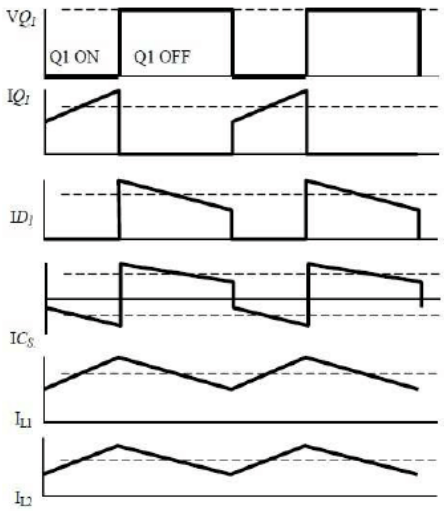

Figure 2.6: Switching Waveforms VQ1:Q1 Drain to source voltage. [27].

2.2.2 Operation And Analysis Of The Non-isolated Switch Mode DC-DC converter

According to the analysis, the fuel cell provides the average power, while the battery and supercapacitor act as energy storage devices to handle power surpluses or shortages. The system is made to match the average power of the load with the high-efficiency operation range of the fuel cell in order to maximize efficiency. In this case, a boost converter is used to raise the DC voltage level while maintaining the appropriate fuel cell size. The power flow between the battery, the supercapacitor, and the load is bidirectional in this case. A bidirectional converter is therefore required.

The following converter topology is suggested, as shown in Figure 2.7, in order to achieve the functionalities and minimize the hardware components. This converter topology may be broken down into two components: a fuel cell boost converter shown in Figure 2.8 and a bidirectional converter shown in Figure 2.9. As the converters used for batteries and supercapacitors are similar, they both work in a similar way; only one converter is explained in detail. Both converters used for this fuel cell hybrid electric vehicle work in continuous conduction mode (CCM).

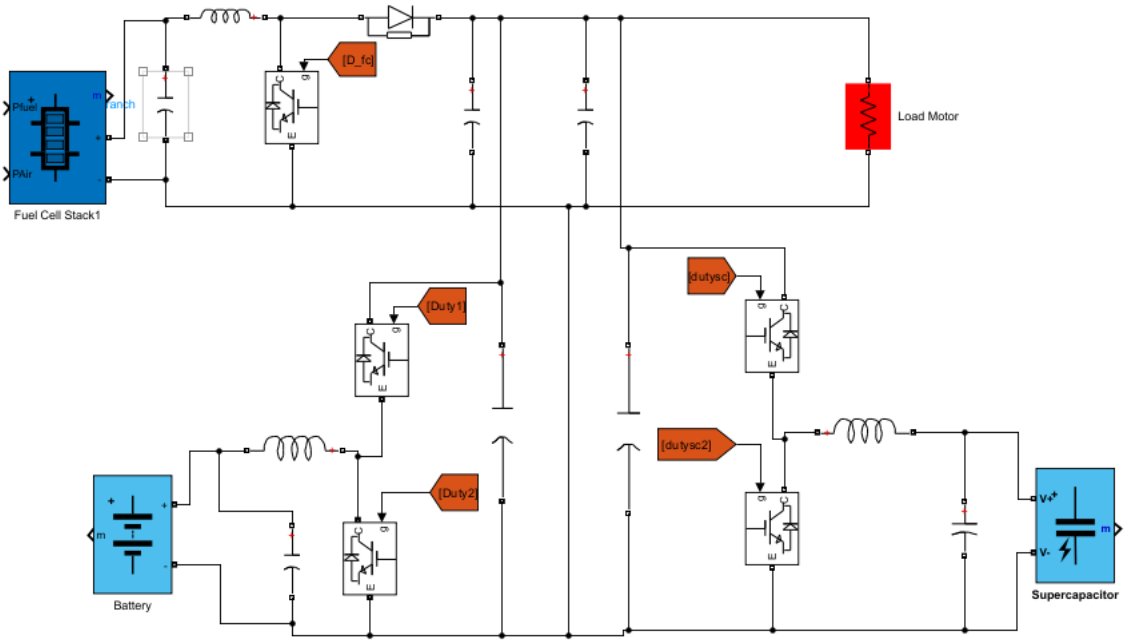

Figure 2.7: Designed Converter For FCHEV Application

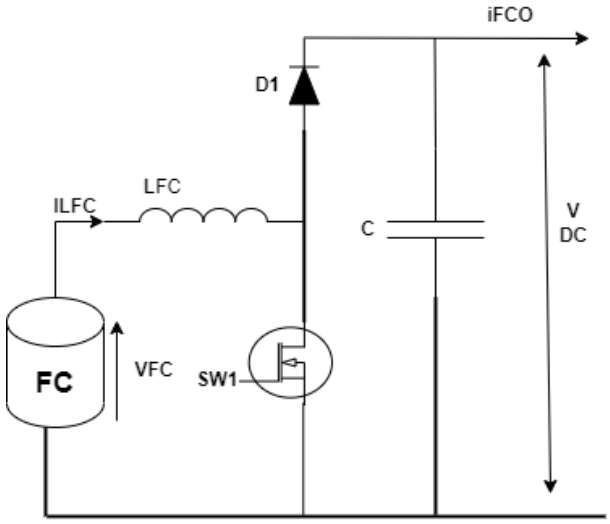

Figure 2.8: Boost Converter For Fuel Cell.

2.2.3 Boost Converter (Fuel Cell)

The fuel cell's boost converter is responsible for keeping the DC bus voltage constant at $30V$. Figure 2.10 shows the converter's circuit diagram when switch §$_1$ is in the ON position (o<t<d_1T_1). The voltage across the diode is currently reverse-biased. A closed circuit is created by the L_{fc} inductor and the fuel cell. Fuel cell voltage is added through the inductor L_{fc}, and the current flowing through it is equivalent to the fuel cell's current. The DC bus current in this converter exclusively comes from capacitor C because the diode current is zero. Through the load, capacitor C is discharged. Thus, the following equations are obtained: For (o<t<d_1T_1)

$$V_{FC} = V_{LFC} \tag{2.24}$$

$$L_{FC}\frac{di_{LFC}}{dt} = V_{FC} \tag{2.25}$$

$$I_L t = \frac{V_{FC}}{L_{FC}}t + I_{L,min} \tag{2.26}$$

$$i_L(t = d_1T_1) = I_{L,max} \tag{2.27}$$

$$\delta I_L = I_{L,max} - I_{L,min} = \frac{V_{FC}}{L_{FC}}d_1T_1 \tag{2.28}$$

The converter's circuit diagram is shown in Figure 2.11 when switch S1 is off (d_1T_1<t<T_1). During this period, the forward-biased diode conducts. Only the diode and the load can get the current from the fuel cell. The fuel cell's current is therefore flowing via the inductor L_{FC}, the diode $D1$, and the load, while there is no current flowing through the switch. The capacitor C and the load are using up the energy that the inductor L_{FC} has stored. The current through L_{FC} is decreasing as the energy in L_{FC} is being used up. The voltage on an L_{FC} is equal to the voltage difference between the load and the fuel cell.

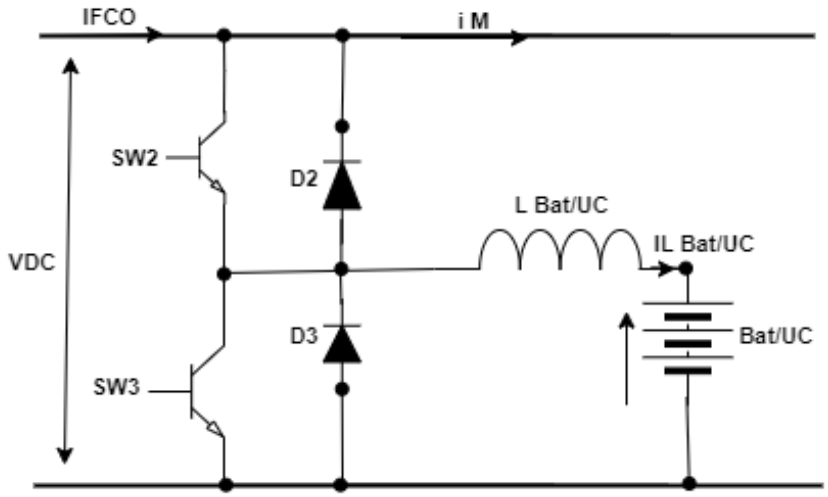

Figure 2.9: bidirectional Converter For Battery and Supercapacitor.

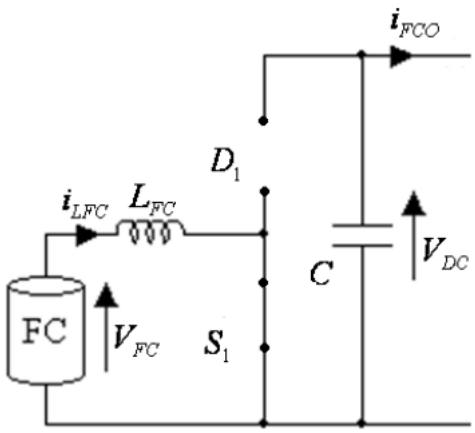

Figure 2.10: Boost Converter Of The Fuel Cell When S_{FC} is ON.

The state equations during this time interval are as follows.

For $(d_1T_1<t<T_1)$,

$$V_{LFC} = V_{Fc} - V_{DC} \tag{2.29}$$

$$L_{Fc}\frac{di_{LFC}}{dt} = -(V_{DC} - V_{FC}) \tag{2.30}$$

$$i_{Fc}(t) = \frac{-(V_{DC} - V_{FC})}{L_{FC}}(t - d_1t_1) + I_{LFC,max} \tag{2.31}$$

$$i_{LFc}(t = T_1) = I_{LFC,min} \tag{2.32}$$

$$\delta I_{LFC} = I_{LFc,max} - I_{LFC,min} = \frac{V_{DC-V_{FC}}}{L_{FC}}(1 - d_1)T_1 \tag{2.33}$$

Since it is operating in continuous conduction mode, a new cycle begins before the inductor current hits zero when switch $S1$ is turned ON. Additionally, the fuel cell's long response time and the converter's high-frequency switching result in a small change in current every cycle. From Equation (2.24) to (2.33), we can get:

$$V_{DC} = \frac{V_{FC}}{1 - d_1} \tag{2.34}$$

Where

$$d_1 = \frac{t_{1on}}{T_1} \tag{2.35}$$

is the duty cycle of the fuel cell boost converter, which typically ranges between 0 to 1.

Figure 2.12 shows the variations of the inductors voltage and current.

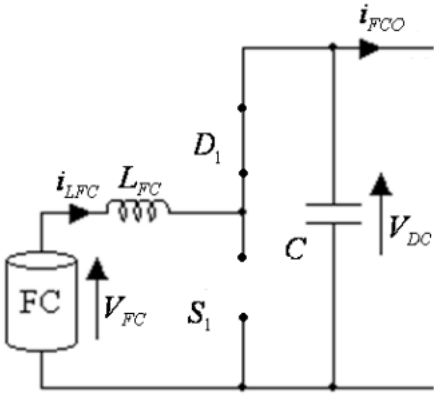

Figure 2.11: Boost Converter Of The Fuel Cell When S_1 is Off

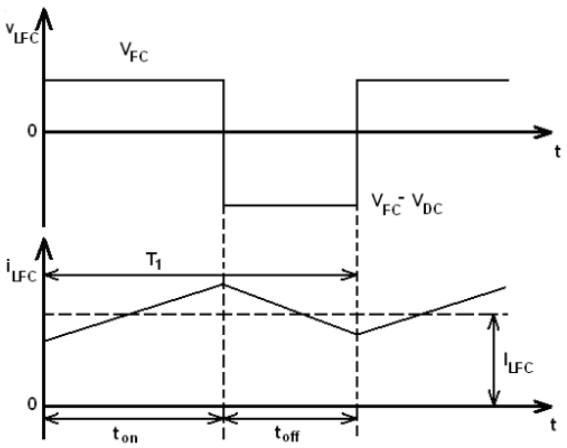

Figure 2.12: Inductor Voltage and Current Of The Fuel Cell Boost Converter.

2.2.4 Bidirectional Buck-Boost Converter at the Battery and Ultracapacitor end

Bidirectional Converter as Buck Converter

The bidirectional converter is used to achieve power balance by managing current flow at the junction of the fuel cell, battery, an ultracapacitor. Figure 2.9 serves as a design for its topology. According to figure 2.13 -2.14, S_2 and D_3 create the bucking pattern from the DC bus to the battery or ultracapacitor, and S_3 and D_3 make up the boost converter from the battery or ultracapacitor to the DC bus. The S_2 and S_3 switches do not complement each other. Because the DC bus voltage is intended to be higher than the voltage of the ultracapacitor, when power is delivered to the battery or ultracapacitor via the DC bus, the buck converter runs while the boost converter does not. The buck converter can step down the DC voltage to the voltage level of the battery or supercapacitor by switching S_2 at particular duty cycles. The boost converter can also stop working if S_3 is left open. The voltage is increased when power is transferred from the battery to the DC bus; as a result, the boost converter operates while the buck converter does not. The boost converter operates similarly to the buck converter mode, with the S_3 flipping in accordance with the predicted duty cycle and the S_2 remaining open to protect the buck converter from this circumstance. The following describes the precise control algorithm of the Bidirectional Converter Connecting the Ultracapacitor or Battery to the DC bus.

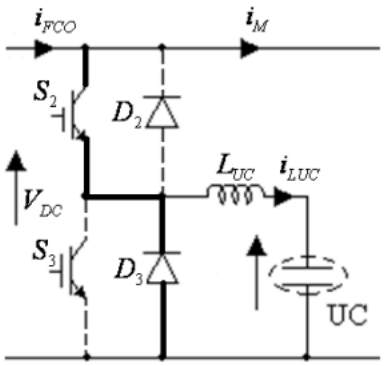

Figure 2.13: Buck Converter From The DC Bus To The Ultracapacitor or Battery.

Figure 2.13 is a representation of the buck mode; it works in the continuous conduction mode (CCM). Following the activation of switch S_2, when ($o<t<d_2T_2$), current flows through the inductor L_{UC} as shown in Figure 2.15. The diode D_3 is forced to experience a negative voltage, making it reverse-biased. The ultracapacitor gets charged from the DC bus when the current flowing through the inductor starts to increase.

For $O<t<d_2T_2$,

$$V_{DC} = V_{LUC} + V_{UC} \tag{2.36}$$

$$L_{UC}\frac{di_{LUC}}{dt} = V_{DC} - V_{UC} \tag{2.37}$$

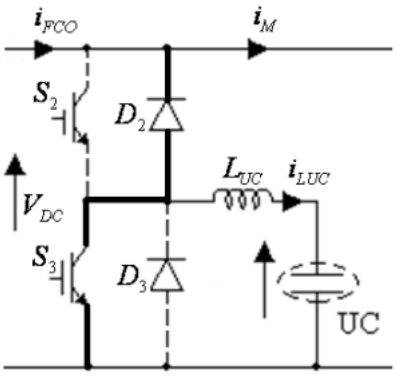

Figure 2.14: Boost Converter From The Ultracapacitor or Battery To The DC Bus.

$$i_{LUC}(t) = \frac{V_{DC} - V_{UC}}{L_{UC}} t + I_{LUC,min} \tag{2.38}$$

$$i_{LUC}(t = d_2 T_2) = I_{LUC,max} \tag{2.39}$$

$$\delta I_{LUC} = I_{LUC,max} - I_{LUC,min} = \frac{V_{DC} - V_{UC}}{L_{UC}} d_2 T_2 \tag{2.40}$$

Figure 2.16 depicts the circuit diagram when switch S_2 is off (d_2T_2<t<T_2). The diode is used to close the loop. Consequently, the current flowing through the inductor drops as the inductor transfers the energy it has stored therein to the ultracapacitor. The amplitude of the negative voltage across the inductor is clamped to the voltage of the ultracapacitor. The following observations are available:

For d_2T_2<t<T_2

$$V_{LUC} = -V_{UC} \tag{2.41}$$

$$L_{UC} \frac{di_{LUC}}{dt} = -V_{UC} \tag{2.42}$$

$$i_{LUC}(t) = \frac{-V_{UC}}{L_{UC}} (t - d_2 T_2) + I_{LUC,max} \tag{2.43}$$

$$i_{LUC}(t = T_2) = I_{LUC,min} = \frac{V_{UC}}{L_{UC}} (1 - d_2) T_2 \tag{2.44}$$

So we get,

$$V_{UC} = d_2 V_{DC} \tag{2.45}$$

where, $d_2 = \frac{t_{2on}}{T_2}$ is the duty cycle of the fuel cell boost converter, which ranges from 0 to 1.

The waveforms of the inductor's current and voltage are shown in the figure below 2.17.

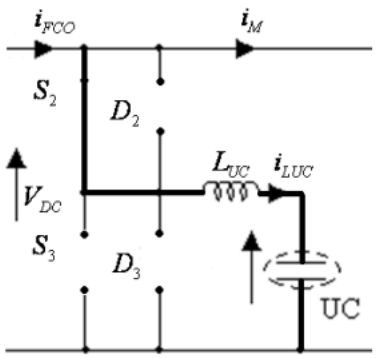

Figure 2.15: Buck Converter From the DC Bus To The Ultracapacitor or Battery When S_2 is ON.

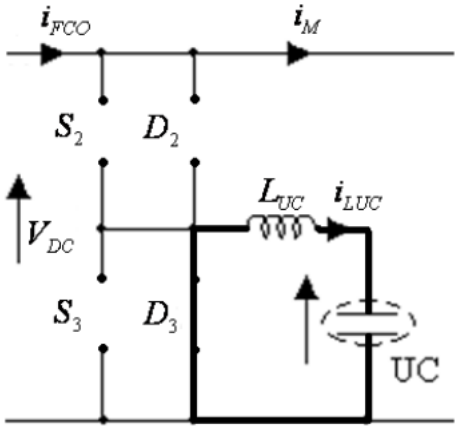

Figure 2.16: Buck Converter From the DC Bus To The Ultracapacitor or Battery When S_2 is OFF.

Equations 2.37 and 2.42 can be stated in the following forms when the switch is used in high frequency.

$$L_{UC}\frac{i_{LUC}[t(n)+d_2(n)*T_2]-i_{LUC}[t(n)]}{d_2(n)*T_2}=V_{DC}[t(n)]-V_{UC}[t(n)] \tag{2.46}$$

$$L_{UC}\frac{i_{LUC}[t(n+1)-i_{LUC}[t(n)+d_2(n)*T_2]}{1-d_2(n)*T_2}=-V_{UC}[t(n)] \tag{2.47}$$

where d_2(n) is the duty cycle of the nth interval, and $t(n)$ and $t(n+1)$ are the interval's start and end times, respectively. According to Figure 49, the inductor current at the start of the nth and $(n+1)th$ switching cycles is represented as $i_{LUC}[t(n)]$,$i_{LUC}[t(n+1)]$. The inductor current i_{LUC} at the time the switch s_2 is turned can be obtained from equation 2.46 as

$$i_{LUC}[t(n)+d_2(n)T_2]=i_{LUC}[t(n)]+\frac{1}{L_{LUC}}V_{DC}[t(n)]-V_{UC}[t(n)]d_2(n)T_2 \tag{2.48}$$

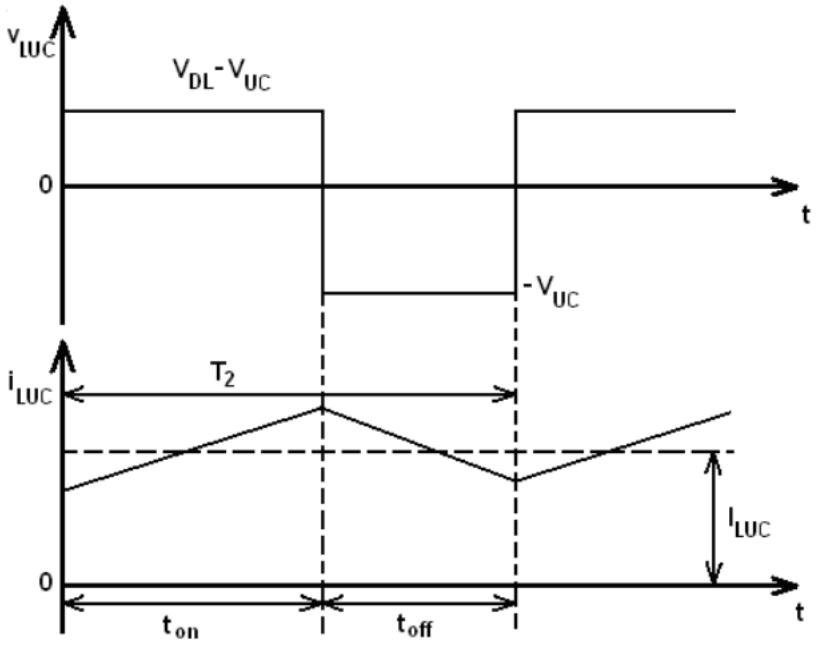

Figure 2.17: Inductor voltage and current of the Boost Converter.

The inductor current I_{LUC} at the time $(n+1)th$ cycle is obtained from equation 2.47 as,

$$i_{LUC}[t(n+1)] = I_{LUC}[t(n) + d_2(n)T_2] - \frac{1}{L_{UC}} V_{UC}[t(n)][1 - d_2(n)T_2] \tag{2.49}$$

substituting Equation 2.48 into Equation 2.49,

$$i_{LUC}[t(n+1)] = I_{LUC}[t(n)] - \frac{1}{L_{UC}} V_{UC}[t(n)]T_2 + \frac{1}{L_{UC}} V_{DC}[t(n)]d_2(n)T_2 \tag{2.50}$$

The discrete form of equation 2.50 is,

$$i_{LUC}(n+1) = i_{LUC}(n) - \frac{V_{UC}(n)T_2}{L_{UC}} + \frac{V_{DC}(n)d_2(n)T_2}{L_{UC}} \tag{2.51}$$

According to the equation above, the current at the start of the current cycle, the voltage across the ultracapacitor, the voltage across the DC bus, and the duty cycle of the current cycle all affect the inductor current i_{LUC} at the start of the following cycle. The duty cycle d_2 can be obtained from equation 2.51,

$$d_2(n) = \frac{L_{UC}}{T_2} \frac{i_{UC}(n+1) - i_{LUC}(n)}{V_{DC}(n)} + \frac{V_{UC}(n)}{V_{DC}(n)} \tag{2.52}$$

Therefore, the converter parameters, input voltage V_{DC}, output voltage V_{UC}, and inductor current L_{UC}, all affect the duty cycle of the current cycle. In order to regulate the power flow between the ultracapacitor and the DC bus, $V_{DC}(n)$ is intended to follow the reference voltage $V_{DCref}(n)$ attributed to the boost converter at the fuel cell end, and $L_{UC}(n+1)$ is designed to follow the

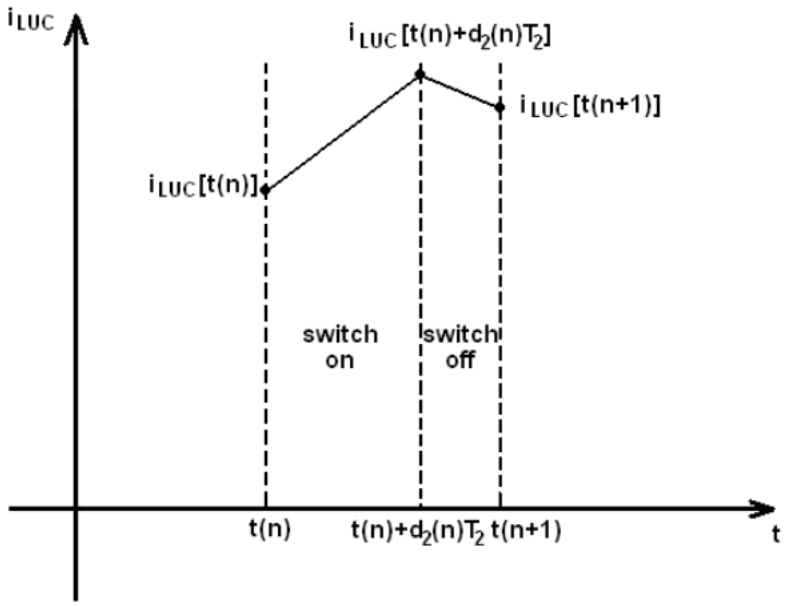

Figure 2.18: Inductor Current I_{LUC} in The nth Cycle.

reference current $L_{UCref}(n+1)$ as shown in Figure 2.19. The reference current $i_{LUCref}(n+1)$ can be obtained from Krichhoffs current law and conservation of power as,

$$i_{LUCref}(n+1) = (i_{fco} - i_M) * \frac{V_{DC}(n)}{V_{UC}(n)} \tag{2.53}$$

Substituting $i_{LUCref}(n+1)$ to get $i_{LUC}(n+1)$ in equation 2.52,

$$d_2(n) = \frac{L_{UCref}}{T_2} \frac{i_{UC}(n+1) - i_{LUC}(n)}{V_{DC}(n)} + \frac{V_{UC}(n)}{V_{DC}(n)} \tag{2.54}$$

Where i_{LUC} and $V_{DC}(n)$ are the input current and voltage at the beginning of the cycle.

Bidirectional Converter as Boost Converter

The boost converter with S_3 and D_2 operates on a similar concept to the fuel cell boost converter with S_1 and D_1. The current flows as shown in Figure 2.20 when switch S_3 is turned on. And when switch S_3 is off, the circuit diagram is shown in Figure 2.21. The ultracapacitor voltage and the DC bus voltage have the following relationship:

$$V_{DC} = \frac{V_{UC}}{1 - d_3} \tag{2.55}$$

Where $d_3 = \frac{t_{on}}{T_3}$ is the duty cycle of S_3, which is ranged from 0 to 1. A few times, compared to the usual bidirectional converter, do s_2 and s_3 switch on simultaneously. As a result, the conversion efficiency is increased while also drastically reducing the conduction losses. Additionally, neither zero voltage switching nor zero current switching is necessary.

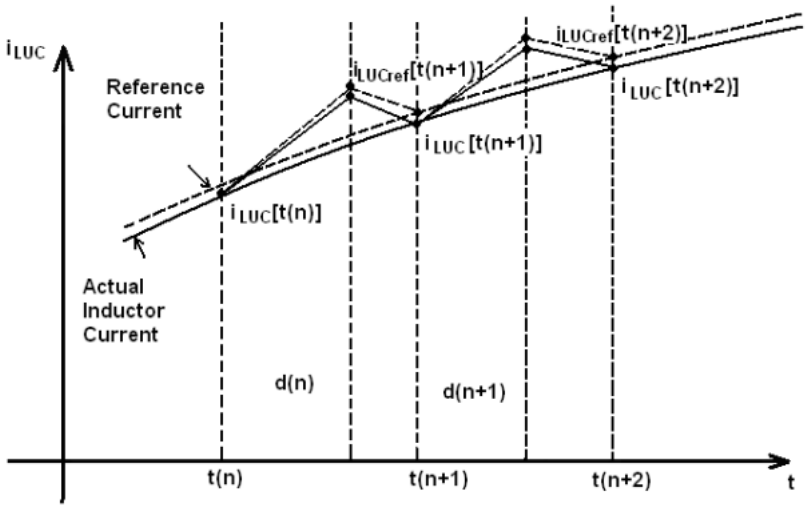

Figure 2.19: Inductor Current Tracking The Reference Current.

Similarly, the following equation can be derived:

$$L_{UC}\frac{i_{LUC}[t(n)+d_3(n)T_3]-i_{LUC}[t(n)]}{d_3(n)T_3}=-V_{UC}[t(n)] \tag{2.56}$$

$$L_{UC}\frac{i_{LUC[t(n+1)]-i_{LUC}[t(n)+d_3(n)T_3]}}{[1-d_3(n)]T_3}=V_{DC}[t(n)]-V_{UC}[t(n)] \tag{2.57}$$

where $d_3(n)$ is the duty cycle of the nth interval, and $t(n)$ and $t(n+1)$ are the interval's start times. The inductor current at the start of the nth and $(n+1)th$ switching cycles is $i_{LUC}[t(n)]$ and $i_{LUC}[t(n+1)]$. The inductor current i_{LUC} at the time the switch s_3 is turned can be obtained from equation 2.56 as:

$$i_{LUC}[t(n)+d_3(n)T_3]=i_{LUC}[t(n)]-\frac{1}{L_{UC}}V_{UC}[t(n)]d_3(n)T_3 \tag{2.58}$$

The inductor current i_{LUC} at the begining of the $(n+1)th$ cycle can be derived from equation 2.57 as:

$$i_{LUC}[t(n+1)]=i_{LUC}[t(n)+d_3(n)T_2]+\frac{1}{L_{UC]}}V_{Dc}[t(n)]-V_{UC][t(n)]}[1-d_3(n)]T_3 \tag{2.59}$$

Substituting Equation 2.58 into Equation 2.59,

$$i_{LUC}[t(n+1)]=i_{LUC}[t(n)]-\frac{1}{L_{UC}}V_{UC}[t(n)]T_3+\frac{1}{L_{UC}}V_{Dc}[t(n)][1-d_3(n)]T_3 \tag{2.60}$$

The discrete form of Equation 2.60 is:

$$i_{LUC}(n+1)=i_{LUC}(n)-\frac{V_{UC}(n)T_3}{L_{UC}}+\frac{V_{DC}(n)[1-d_3(n)]T_3}{L_{UC}} \tag{2.61}$$

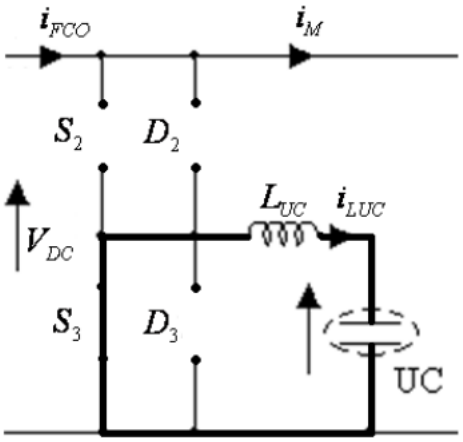

Figure 2.20: Boost Converter From Battery To Dc Bus When S_3 is ON.

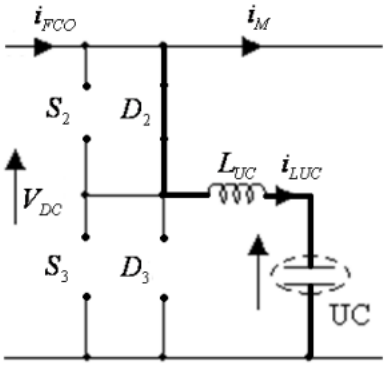

Figure 2.21: Boost Converter From The Battery To The Dc Bus When S_3 is OFF.

According to the equation above, the current at the start of the current cycle, the voltage across the ultracapacitor, the voltage across the DC bus, and the duty cycle of the current cycle all affect the inductor current i_{LUC} at the start of the following cycle. Equation 2.61 can also be used to get the duty cycle d_3.

$$d_3(n) = -\frac{L_{UC}}{T_3}\frac{i_{LUC}(n+1) - i_{LUC}(n)}{V_{DC}(n)} + \frac{V_{DC}(n) - V_{UC}(n)}{V_{DC}(n)} \tag{2.62}$$

Therefore, the converter parameters, input voltage V_{DC}, output voltage V_{UC}, and inductor current i_{LUC}, all affect the duty cycle of the current cycle.

To control the power flow between the battery and supercapacitor and the DC bus, $i_{LUC}(n+1)$ is required to follow the reference current $i_{LUCref}(n+1)$ which will track the reference voltage $V_{DCref}(n)$ coming from the boost converter at the Fuel Cell end. Where $i_{LUCref}(n+1)$ is given as:

$$i_{LUCref}(n+1) = (i_{FcO} - i_M) * \frac{V_{DC}}{V_{UC}} * V_{DC}(n) \tag{2.63}$$

Substituting $i_{LUCref}(n+1)$ to $i_{LUC}(n+1)$ in Equation 2.62,

$$d_3(n) = -\frac{L_{UC}}{T_3}\frac{I_{LUC_{ref}}(n+1) - i_{LUC}(n)}{V_{DC}(n)} + \frac{V_{DCref}(n) - V_{UC}(n)}{V_{DC}(n)} \tag{2.64}$$

In order to achieve maximum system efficiency, the forward control approach suggested above can manage the current of the Fuel Cell and the Battery and Ultracapacitor as well as the voltage of the DC bus.

3

Fuel Cell Simulation and Converter Modelling

A fuel cell hybrid electric vehicle is made up of two main subsystems: the fuel cell system and the energy storage system (battery and supercapacitor/ultracapacitor), as explained in Section 1.2.3. A systematic approach is needed for system modeling. As explained in Section 2.1 a mathematical model of the system represents its properties and reflects its dynamic and static behavior. It offers a straightforward explanation of how the system is operated through a demonstration. In order to provide the electricity needed to satisfy the load demand, the fuel cell system, and the power conversion system are first individually modeled. The power equation for the controller design is then formulated after a detailed analysis of the modeling of the two systems in this chapter.

3.1 Fuel Cell System Simulation

Various subsystems make up a comprehensive fuel cell system, as mentioned in [10] and Figure 1.5. The fuel cell model must be able to balance robustness, authenticity, and computing effort in order to accurately build the controller. A fuel cell system model can typically be built on two models:

- one that maps the system efficiency and net power output to the entire fuel cell system,
- one in which the polarization curve indicates the corresponding hydrogen consumption and the number of cells in the stack [28].

The MATLAB/SIMULINK model is presented in Appendix *B*. In this section, the result of the simulation is presented briefly. Figure 3.1 shows the polarization curve of the *PEMFC* for the given parameters shown in Table 2.1. When the electrical energy is drawn from the fuel cell, the actual cell voltage drops from the theoretical voltage due to several losses. The various losses are defined below and can be seen in Figure 3.1. The actual voltage of a fuel cell is lower than the ideal Nernst potential. The curve starts at the maximum value, i.e., slightly below the ideal voltage. The three potential losses are the causes of the voltage drop. During low current density, the activation loss is the cause for the decrease in the graph. The linear portion in the middle shows the losses due to ohmic losses. The considerable drop, in the end, describes the concentration losses. The total voltage of the fuel cell drops with increasing current density, as can be seen from the polarization curve.

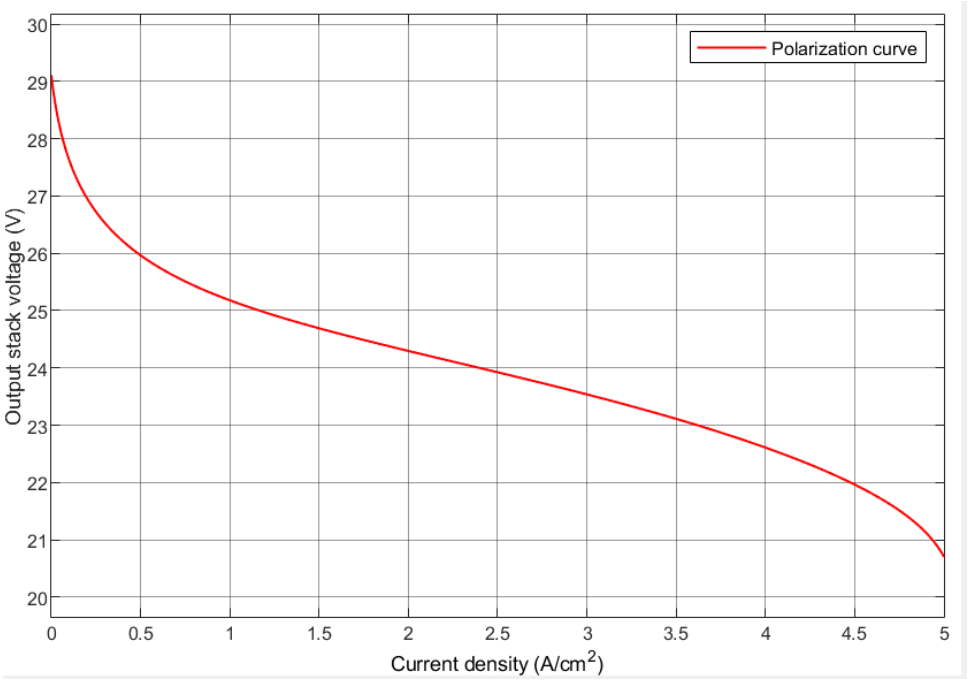

Figure 3.1: Polarization curve of fuel cell

figure 3.2 represents the ideal cell voltage. The graph displays a straight line, which means that the output voltage is constant and does not change depending on the current density. This graph will be realized if the cell were to function in a lossless environment.

The steady-state activation losses against current density are shown in Figure 3.3. It is clear that at lower current densities, activation losses predominate and there is initially a dramatic reduction in current density. This is because of the slow start of the reaction. Additionally, the initial voltage output is the cause of the activation energy of the reaction. The activation losses are influenced by the oxygen content since the reaction at the cathode, which involves the reduction of oxygen and the creation of water, is a slow one.

The graph of ohmic losses vs current density is shown in Figure 3.4. The ohmic losses graph is linear. The resistance provided by the fuel cell components rises as the reaction proceeds and the

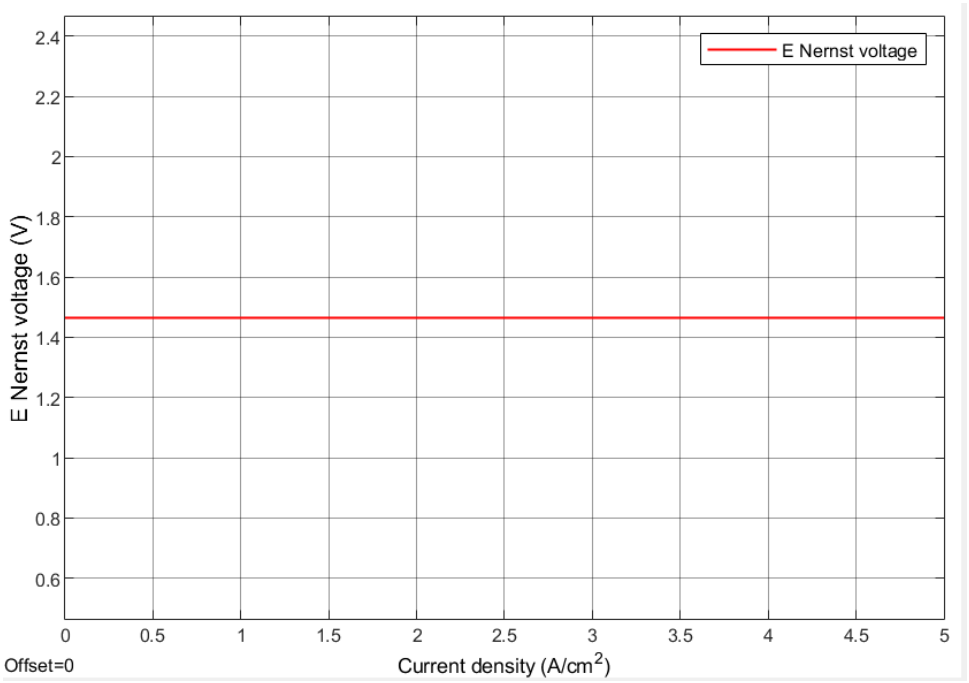

Figure 3.2: Ideal Cell Voltage (E nernst Potential)

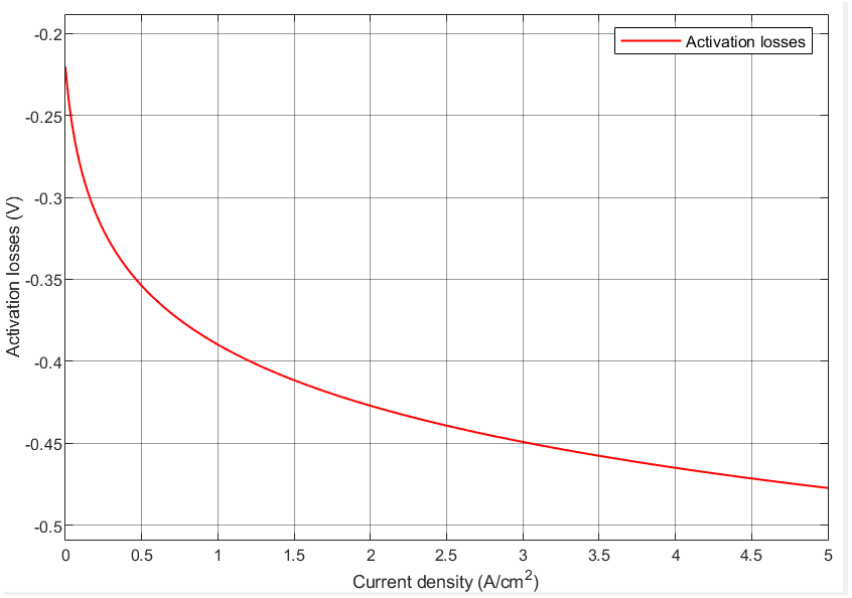

Figure 3.3: Activation Losses

current density rises. The ohmic loss is mainly caused by the resistances of the wire, the bipolar plate, and the proton exchange membrane.

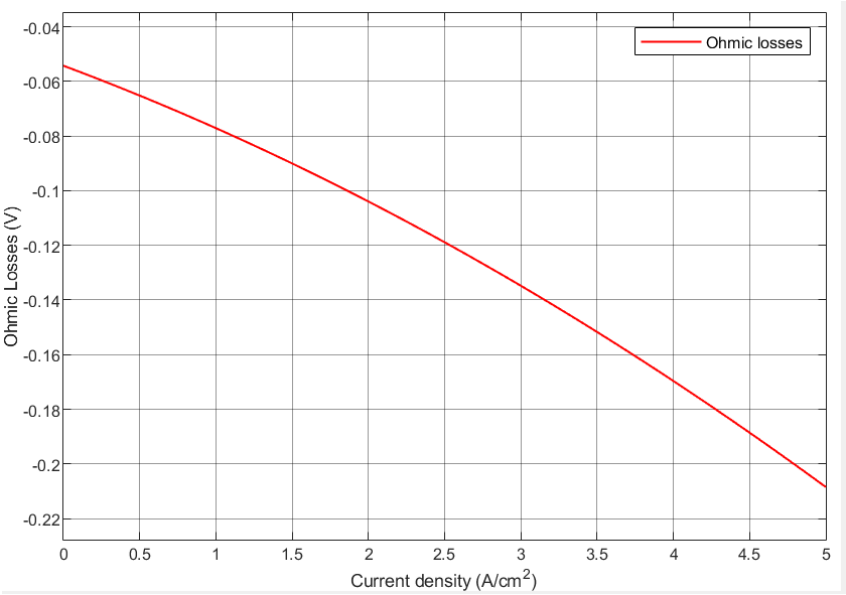

Figure 3.4: Ohmic losses.

The concentration losses that occur near the polarization curve's end are represented in Figure 3.5. These losses can be shown to grow as the current density increases. At the point where the limiting current occurs, a drastic drop in voltage can be seen. When the current being drawn from the fuel cell rises above the limiting current, the fuel being consumed becomes greater than the fuel being supplied, at this point the fuel cell stops working and the voltage drops rapidly.

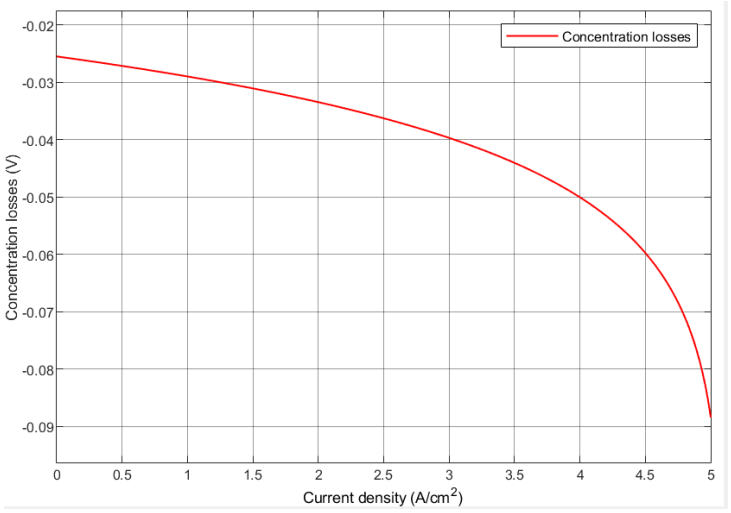

Figure 3.5: Concentration losses.

Figure 3.6 shows the power output of the PEMFC. The power can be obtained by the product of the input current and output voltage. The power output shows an increasing trend up to a value that is limited by limiting current and increasing the current beyond this value results in a fall in output power as can be seen in the figure 3.6. This is because as the input current approaches the limiting current the power output starts to decrease because the concentration losses start to decrease at this point.

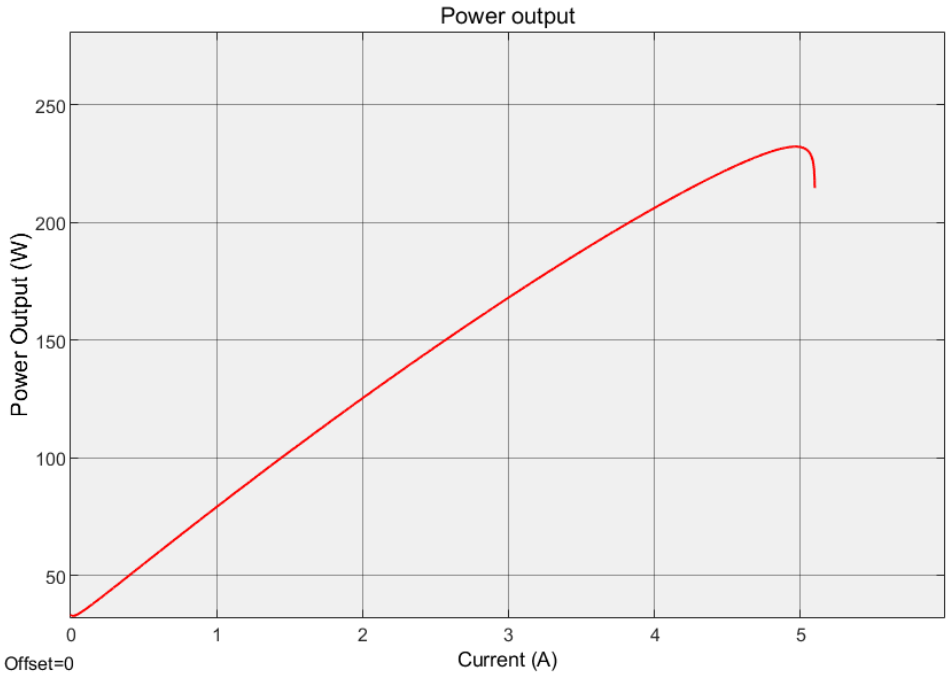

Figure 3.6: Power output of the stack.

3.2 Converter Modelling

In this thesis, a non-isolated switch-mode DC-DC converter is chosen to study, as indicated in Chapter [2]. This chapter provides detailed illustrations of the converter design process for both the battery and supercapacitor bidirectional converter and the fuel cell converter. With the exception of slight variations in the values of the capacitor and inductor, the converter used for the supercapacitor and battery will be the same. The control algorithm used for the entire hybrid system is then explained.

3.2.1 Boost Converter For Fuel Cell System

The possible switch and Mosfet-diode arrangements are shown in Figure 2.8. This topology is known as a boost converter since the output voltage is higher than the input, as will be shown in this section. In this section, the converter design procedure is illustrated with a converter that

is fed from the fuel cell whose controller characteristics are described in the next chapter. The input voltage $V_{FC,min} = 8.4V$ to $V_{FC,max} = 12V$, fixed output voltage (DC bus voltage) $V_{DC} = 30V$, output power $P_{DC} = 30w$, and switching frequency $f_s = 25KHz$.

The duty cycle of the fuel cell boost converter is derived from,

$$D = 1 - \frac{V_{FC}}{V_{DC}} \tag{3.1}$$

For continuous conduction mode, the inductance minimum value is given by:

$$L_{crit} = \frac{R * T}{2}(1 - D)^2 D \tag{3.2}$$

Where the time period is calculated by:

$$T = \frac{1}{fs} \tag{3.3}$$

and Resistance is given by: $R = \frac{V_o^2}{P_o}$.

The value of the inductor is chosen is chosen so that it is higher than L_{crit}, for continuous conduction mode operation. The output voltage ripple is:

$$\frac{\Delta V_o}{V_o} = \frac{D}{R * C * fs} \tag{3.4}$$

The capacitor value is calculated from equation 3.4, where the output ripple voltage $\frac{\Delta V_o}{V_o}$ is assumed to be 2 percent.

3.2.2 Bidirectional Buck-Boost Converter For Energy Storage System

In order to meet the requirements, this thesis suggests 30 volts. A non-isolated bidirectional DC-DC converter for the battery and ultracapacitor/supercapacitor energy storage components of fuel cell hybrid electric vehicles is selected as shown in figure 2.7. The DC bus is intended to operate at a voltage of 30V. Electrical separation is not necessary at this voltage level. As a result, converters are used to connect the fuel cell, battery, and supercapacitor to the DC bus. The fuel cell and energy storage devices' current ripple is minimized with greater frequency, extending the life of the device, while switching power loss increases. As a result, 20 kHz was chosen as the frequency for all the switches. Accordingly, power MOSFETs are chosen for their ability to switch current at high rates and low ON resistance.

The duty cycle of the converter is derived as:

$$D = \frac{(V_{out} - V_{in})}{V_{out}} \tag{3.5}$$

The inductor ripple current is derived from the Equation:

$$\Delta I_L = 0.01 * I_{out,max} * \frac{V_{out}}{V_{in}} \tag{3.6}$$

Where, $I_{out,max} = \frac{p}{V_{out}}$.

output voltage ripple $\frac{\Delta V_o}{V_o}$ is considered to be 0.01 percent

The value for the inductor and capacitor is calculated from the following equations:

$$L = \frac{(V_{in} * (V_{out} - V_{in}))}{(DeltaI_L * f_s * V_{out})} \tag{3.7}$$

$$C = \frac{(V_{in} * (1 - \frac{V_{in}}{V_{out}})}{(f_s * DeltaV_{out})} \tag{3.8}$$

Note: The values of the inductor and capacitor calculated theoretically may differ from the simulated values due to limitations and constraints within the system.

4

Controller Strategy and Modeling

4.0.1 Control Strategy For Fuel Cell Battery Hybrid system

MPPT Controller For Fuel Cell Boost Converter

The Maximum Power Point Tracking ($MPPT$) control system of the $PEMFC$ with boost converter is shown in Figure 4.1, and it is primarily made up of the $PEMFC$, boost converter, $MPPT$ controller, PWM generator, and external load resistance. The Boost converter is employed in the system to increase the output voltage and as a regulator to implement the $MPPT$ control scheme since it has the benefits of a simple structure, simple control, and voltage amplification. The boost converter's ON and OFF states are controlled by a sequence of square waves with varying duty cycles that are produced by the PWM generator. The PWM controller's output duty cycle is denoted by the letter D.

For the system presented in figure 4.1, the equivalent load resistance of the fuel cell can be derived as:

$$R_{eq} = \frac{U}{I} = (1 - D)^2 * R_L \tag{4.1}$$

Where R_{eq} is the equivalent load resistance of the PEM fuel cell, and R_L is the actual load resistance, which is the load resistance at the output of the boost converter.

It is known that an electric source can only produce its maximum output power if and when it's internal resistance and external resistance are equal. Equation 4.1 states that changing the duty cycle of the boost converter will accomplish the goal of modifying the equivalent load resistance. Therefore, to meet the goal of maximum power output, the duty cycle can be adjusted to bring the PEM fuel cell's equivalent load resistance to its internal resistance [29].

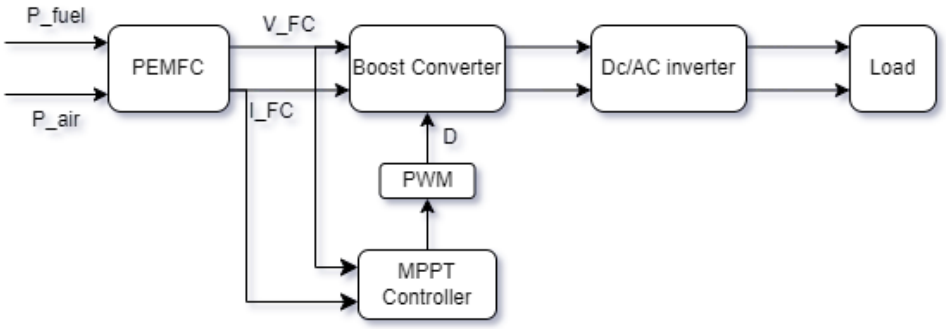

Figure 4.1: Diagram of MPPT Control System.

Perturb and Observe P&O Algorithm

The MPPT method currently utilized most frequently is p&O. The fuel cell is subjected to a positive disturbance voltage in order to sample its output voltage and current and determine the rate at which its voltage and power are changing. If the output power grows following the disturbance, it means that the direction of the voltage that caused the disturbance is also the direction in which the output power is increasing. If not, the disturbance should continue in the opposite direction. To implement the $MPPT$, the disturbance voltage is continually delivered to the fuel cell in accordance with the changing directions of the voltage and power up until the maximum output power is gradually approached. P&O offers the benefits of straightforward calculations and straightforward implementation, but it is only able to maintain the system's oscillations intermittently close to the maximum power point and is unable to precisely track the maximum power point, making it ineffective for addressing the issues of tracking precision and speed [30]. The flowchart of the P&O is shown in figure 4.2, where denotes the duty cycle and ΔP denotes a change in power, $\Delta V and \Delta D$ represents the change in voltage and change in duty cycle.

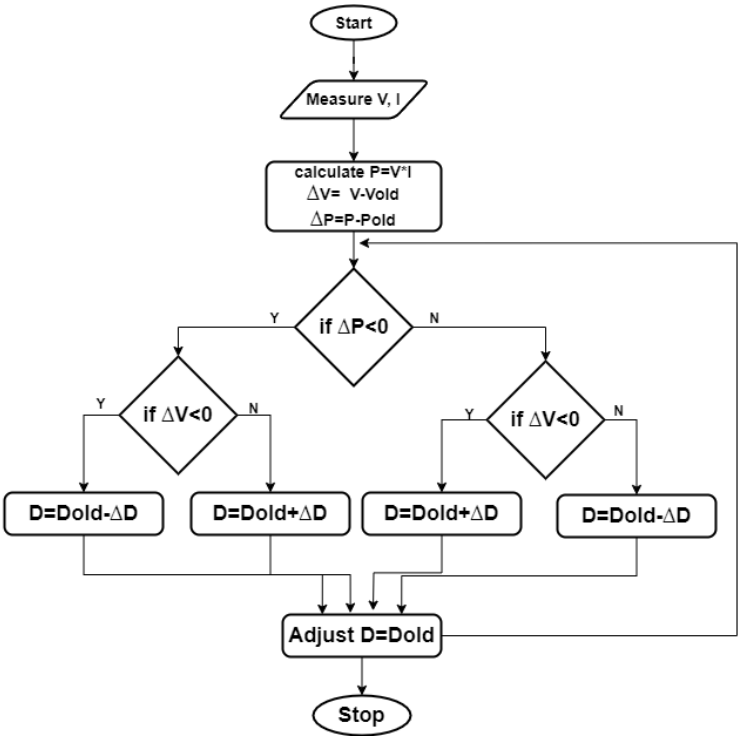

Figure 4.2: Flowchart of PO Algorithm.

PI Controller for Battery Bidirectional Converter

In this thesis, The PI control technique is implemented for the operation of a bidirectional converter which is shown in figure 4.3. In the given scenario, the PI controller is utilized to regulate the charging and discharging of a bidirectional $DC-DC$ converter connected to a battery and a DC bus. The load voltage is influenced by controlling the air and hydrogen flow pressure of the fuel cell. The reference voltage for the PI controller is the desired load voltage, which remains constant at 30 volts.

Initially, when both the hydrogen and air flow pressures of the fuel cell are set to 1, the battery is being charged while the fuel cell is supplying power to the load. The PI controller continuously compares the reference load voltage with the actual load voltage and generates an error signal accordingly.

The PI controller uses this error signal to adjust the duty cycle of the pulse-width modulation (PWM) signal generated by a PWM generator. The duty cycle determines the on-time of the PWM signal, which controls the charging and discharging of the bidirectional $DC-DC$ converter. When the signals are applied to switch $S1$ in the bidirectional $DC-DC$ converter, the converter functions in boost mode, and switch $S2$ acts as a diode. Conversely, when the pulses are provided to switch $S2$, the converter operates in buck mode, and switch S1 functions as a diode as shown in figure (4.4, 4.5).

The output of the PWM generator is then used to control two switches in the bidirectional

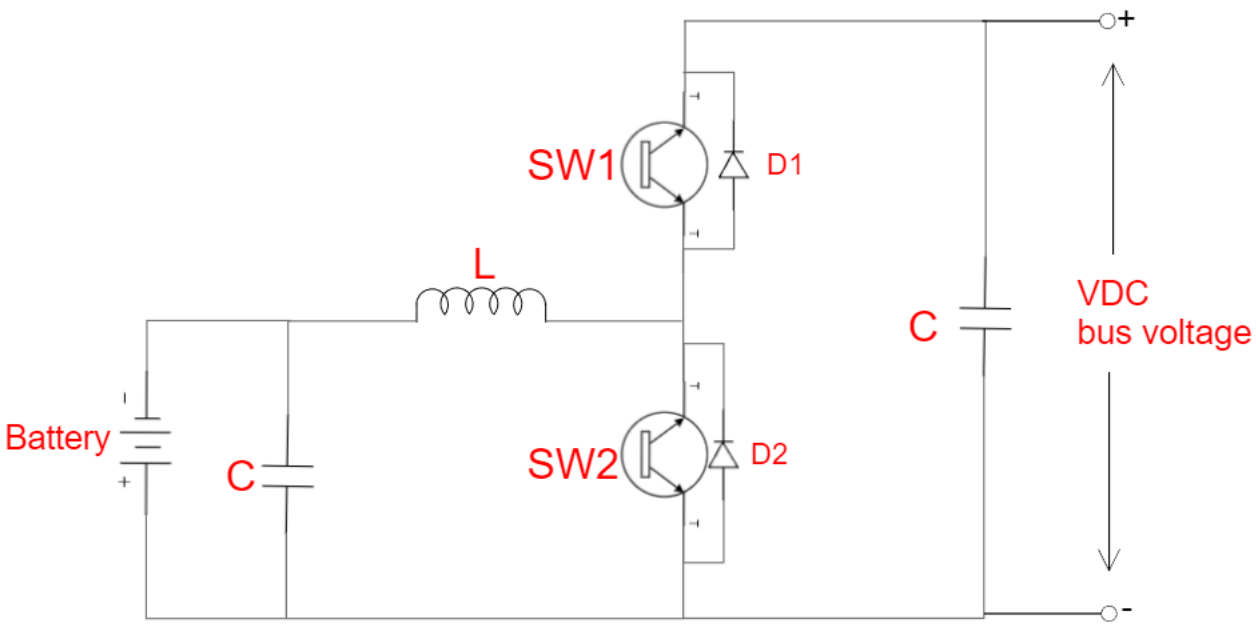

Figure 4.3: Bidirectional Converter.

converter. Switch (SW1) is connected through a NOT gate, while the switch (SW2) is connected directly without a NOT gate. This arrangement allows for bidirectional power flow in the converter, enabling both charging and discharging operations as shown in Figure 4.6.

After 5 seconds, the hydrogen and air flow pressures of the fuel cell are changed to 0.01. This alteration results in a decrease in the output voltage of the fuel cell, causing the actual load voltage to drop below the reference voltage. Consequently, the fuel cell is no longer able to supply sufficient power to the load.

To address this change, the *PI* controller adjusts the duty cycle of the *PWM* signal in response to the new error signal. The duty cycle is reduced to limit the power flow from the battery to the load. As a result, the battery takes over the responsibility of supplying power to the load, compensating for the decreased output voltage of the fuel cell.

Throughout the operation, the *PI* controller continuously monitors the load voltage and modifies the duty cycle accordingly. This ensures that the actual load voltage remains close to the reference voltage, adapting to variations caused by changes in the fuel cell's output voltage resulting from adjustments in the air and hydrogen flow pressure.

By effectively controlling the bidirectional $DC - DC$ converter through the PI controller and the PWM signal, the system maintains stability and efficient operation. The controller enables a seamless transition between charging and discharging modes while adapting to changes in the fuel cell's performance characteristics due to variations in the air and hydrogen flow pressure. The results are explained in the next chapter Simulation and Experimental Results.

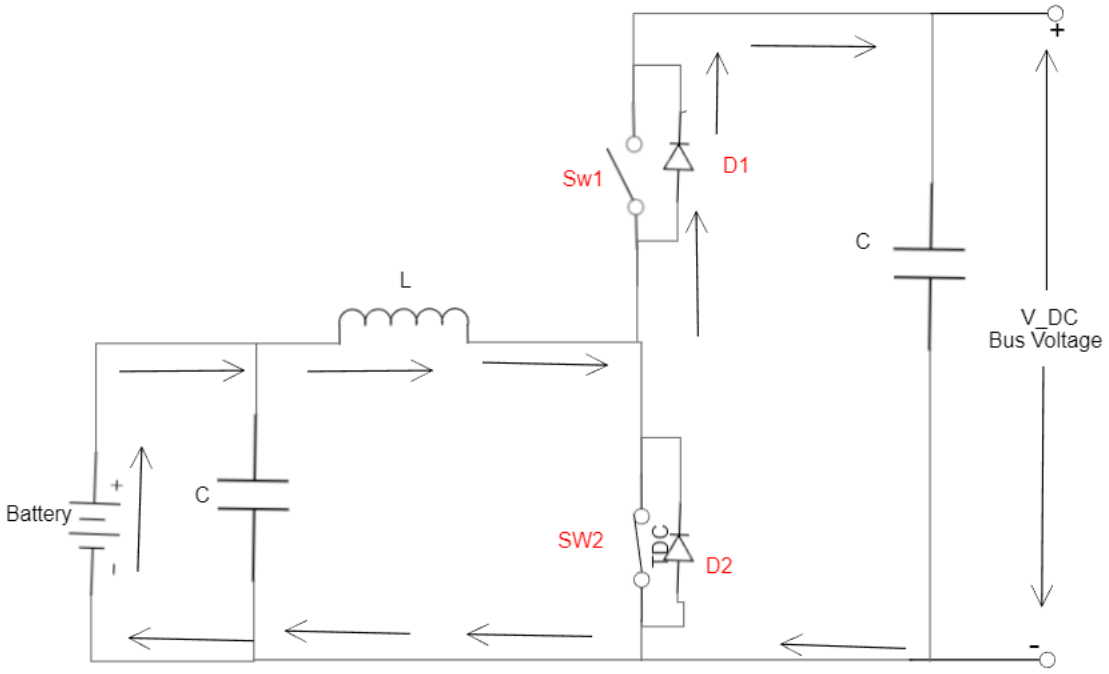

Figure 4.4: Bidirectional Converter Boost Mode (Discharging).

4.1 Control Strategy For Fuel Cell Battery Supercapacitor Hybrid System

4.1.1 MPPT Controller for Fuel Cell Converter

The Maximum power point tracking ($MPPT$) control system is shown in figure 4.7. The MPPT approach finds the operating point that generates the most power. The Maximum Power Point (MPP) is the location where power is generated at the highest rate. To achieve maximum power, $MPPT$ either raises or lowers the operating voltage [31]. The $MPPT$ operates by sensing photovoltaic current and voltage. The $MPPT$ algorithm will process currents and voltages and create a duty cycle that can provide electricity at the Maximum power point. The Duty Cycle will regulate when the converter is turned on. To obtain the most power, $MPPT$ will function in accordance with its algorithm. The switching on of the converter will be controlled by a duty cycle created by the $MPPT$ algorithm. When a Fuel Cell system's power output ($Pload$) exceeds that of the load, the converter will use the excess energy and no longer generate power. When the load power ($Pload$) and the power generated by the fuel cell are equal, no power is generated. The supercapacitor will provide electricity to make up for the shortage of energy when the power generated by the fuel cell system is less than the load power ($Pload$). This hybrid system will still be able to function if one of the input voltages is unable to supply voltage. Therefore, it is predicted that a hybrid energy storage system using the $MPPT$ $P\&O$ algorithm will increase the efficiency of the power generated so that the system's output power is more optimal.

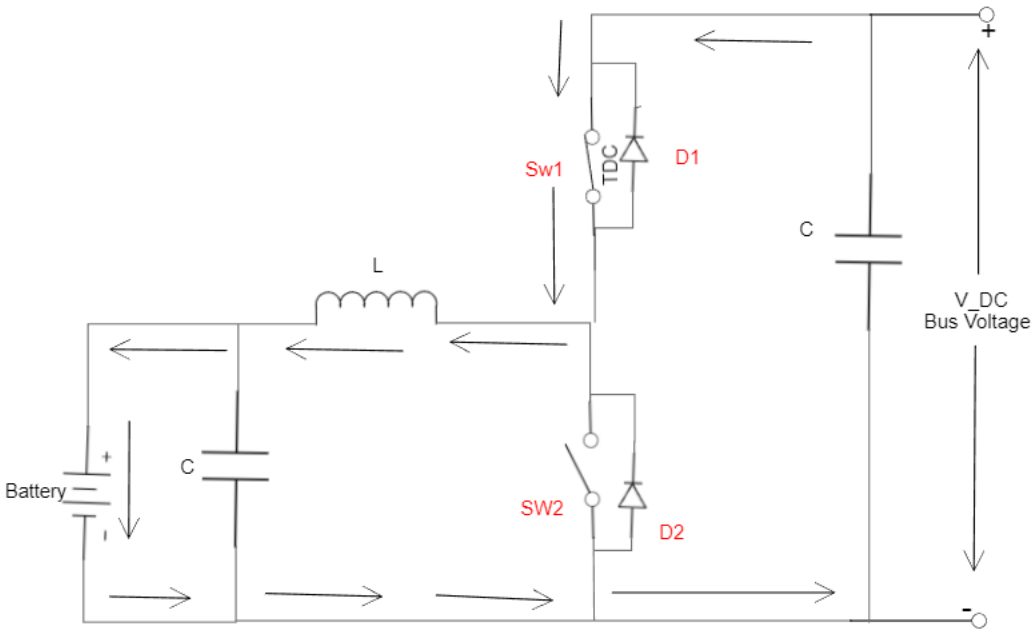

Figure 4.5: Bidirectional Converter Buck Mode (Charging).

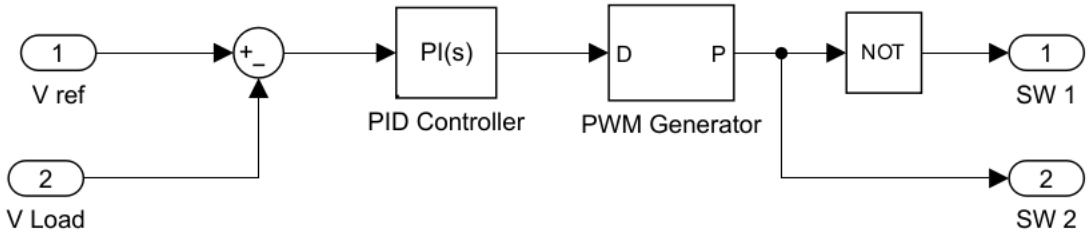

Figure 4.6: Proposed PI Controller.

Perturb and Observe Algorithm (P&O)

The Maximum Power Point *MPP* algorithm, which uses perturbation and observation (P&O), is rarely used in fuel cell systems. However, this method can be applied to fuel cell systems and does not require knowledge of energy storage system parameters. The P&O method's drawback is that steady-state conditions oscillate as a result of the continuous duty cycle adjustments. The system's output power changes as a result of the perturbation in this procedure. The voltage must be increased if disturbances rise as it approaches the maximum power point. Additionally, the voltage must be lowered if the perturbation decreases away from the point of greatest power. This causes the duty cycle to alter as well, and the cycle is repeated until the maximum power point is reached [31]. The flowchart of the algorithm is shown in figure 4.8

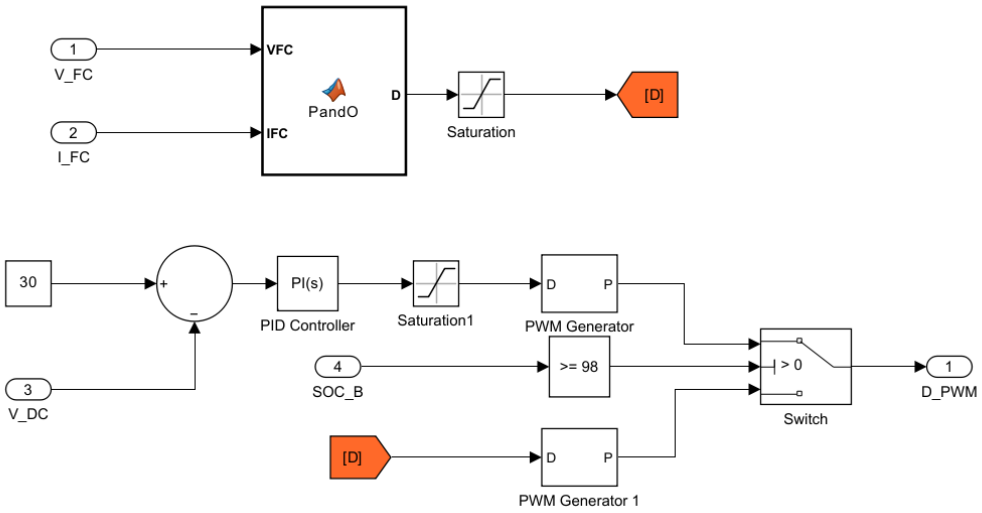

Figure 4.7: Perturb and Observation Based MPPT Algorithm For Energy Optimization.

4.1.2 Proposed Control Strategy

The block diagram for the proposed control technique is shown in Figure 4.9. This algorithm's goal is to reduce the stress that charging and discharging put on batteries, extending their lifespan. Throughout the work, it is assumed that the state-of-charge SOC of the energy storage components is within acceptable limits. In this algorithm, the reference voltage V_{ref} and the average dc bus voltage V_{DC} are compared, and the proportional-integral (PI) controller is provided with the error. The total current needed I_{totref} is produced by the PI controller using an energy storage system. The low-frequency I_{LFref} and high-frequency I_{HFref} components of this I_{tot} ref are separated. The low-frequency component is given as:

$$I_{LFref} = F_{LPF} * I_{totref} \tag{4.2}$$

Here, f_{LPF} represents the low-pass filter's function. The rate limiter receives the low-frequency component to regulate the battery current's charge and discharge rates, i.e., to supply the battery with the reference current as shown below:

$$I_{bref} = F_{RL} * I_{LFref} \tag{4.3}$$

where F_{RL} is the rate limiter's function. The actual battery current I_B is compared to the I_{bref}, and the difference is given to the PI controller as an error. The pulse width modulation PWM generator receives the duty ratio D_{bat} from the PI controller in order to produce switching pulses corresponding to battery switches $SWb1$ and $SWb2$.

The high frequency component I_{totref} and I_{HFref} is given as:

$$I_{HFref} = I_{totref} - I_{bref} \tag{4.4}$$

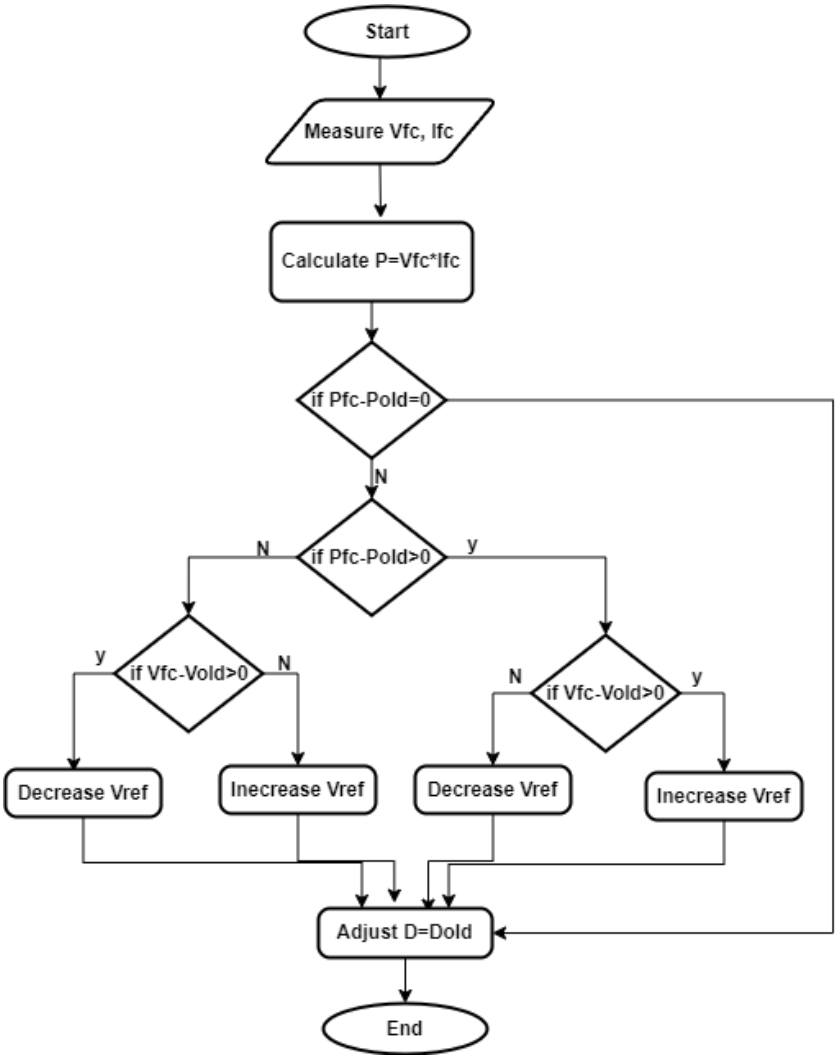

Figure 4.8: Flowchart of Algorithm.

The battery may take some time to track the I_{bref} reference due to the slow dynamics. The uncompensated battery power is therefore presented as:

$$P_{Buncompensated} = I_{HFref} + I_{berror} * V_{Bat} \tag{4.5}$$

Where V_{Bat} is the battery voltage. This uncompensated battery power is then compensated by a supercapacitor. Therefore the reference current of the supercapacitor is given as:

$$I_{sref} = \frac{P_{Buncompensated}}{V_{SC}} = I_{HFref} + I_{berror} * \frac{V_{Bat}}{V_{SC}} \tag{4.6}$$

Where V_{SC} is the supercapacitor voltage. This reference current I_{sref} is compared with the supercapacitor current I_{SC}, and the error is given to the PI controller. The PI controller then generates the duty cycle which is given to PWM generator to generate the switching pulses corresponding to supercapacitors switches $SWsc1$ and $SWsc2$ respectively.

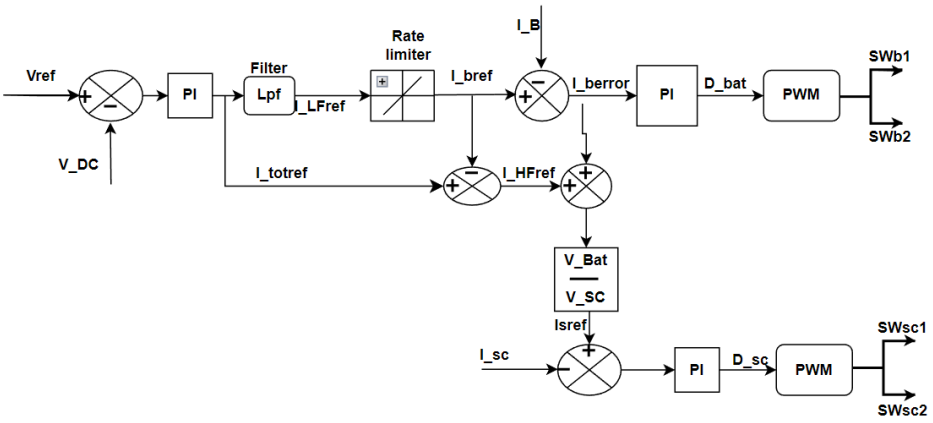

Figure 4.9: Proposed Control Strategy For Hybrid Energy Storage System.

5

Simulation Results

5.1 Fuel Cell, Battery, Hybrid System Model

The circuit diagram shown in figure 5.1 shows that the fuel cell side converter is the boost converter and it is unidirectional. The battery-side converter is the bidirectional converter (BDC) which allows the current to move in both directions. As the bidirectional converter is connected to the battery so during discharging of the battery the bidirectional converter will work in a boost mode. On the other hand, the bidirectional converter will work in buck mode when it is required to charge the battery.

The simulation model for the fuel cell and battery energy storage systems for hybrid electric vehicles is presented in Figure 5.2. In order to get the most power out of the fuel cell, the system comprises a fuel cell stack that is connected to a DC bus or DC load via a boost converter that is controlled by a maximum power point tracker ($MPPT$) P&0 controller. The DC bus is connected to the battery storage system by a bidirectional DC converter, which is managed by a voltage PI controller to keep the DC bus voltage at 30 volts.

The fuel cell can produce $15.7 volts$ and around $1.88 kilowatts$ at its nominal operating point, according to its rating represented by Figure 5.3. The fuel cell runs at $13 volts$ and can produce up to 2600 watts of power at a current of 200 amps. The DC bus, which maintains a voltage of 30 volts, is connected to it. These specifications are used when designing the inductor and capacitor for the boost converter. The battery in use has a $15 - volt$ rating, a $150 - amp - hour$ capacity, and a 75% initial state of charge. The battery converter uses the same inductor and capacitor values as the fuel cell boost converter.

A P&O $MPPT$ algorithm that uses the voltage and current of the fuel cell controls the boost converter. Based on these inputs, the algorithm calculates the power, change in voltage, and change

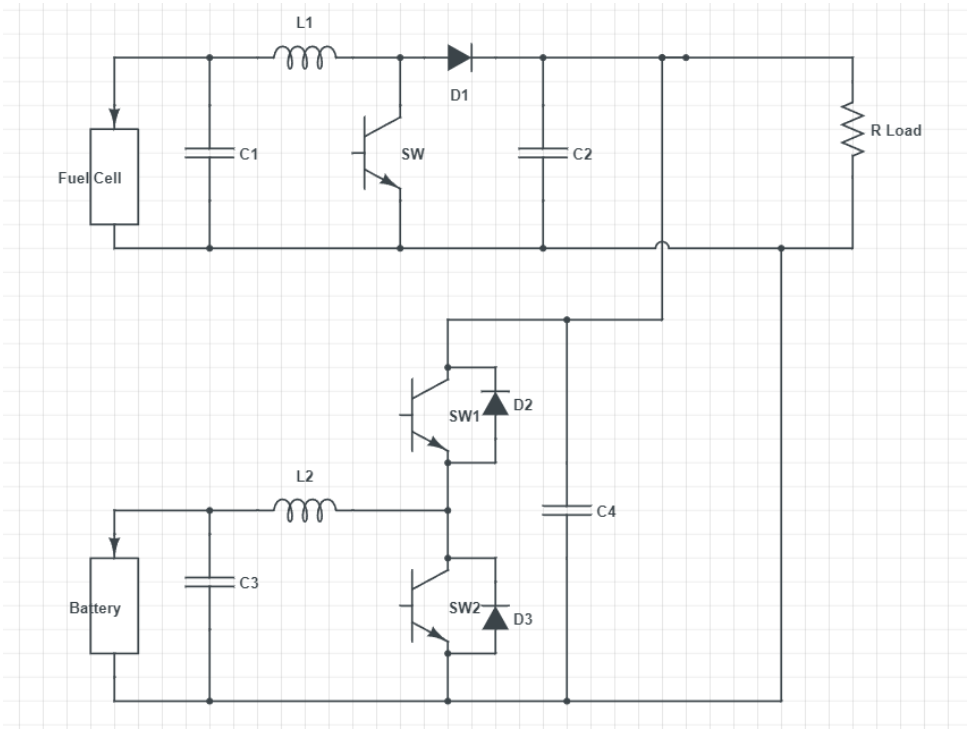

Figure 5.1: Circuit Diagram Of Fuel Cell Battery Hybrid System

in power, and finally outputs the duty cycle for the boost converter. A PWM generator processes the duty cycle produced by the P&O $MPPT$ algorithm, controlling the $MOSFET(Switch)$ connected to the boost converter for maximum fuel cell power output.

A bidirectional $DC-DC$ converter is used to link the battery to the DC bus. The voltage control method is used to control this converter. To maintain the DC bus voltage, the observed load voltage is compared to a $30-volt$ reference voltage. A PI controller processes the difference between the reference voltage and load voltage to produce the duty cycle for the converter. The two MOSFETs are controlled by the PWM generator using this duty cycle to maintain the DC bus voltage at $30volts$. The resistance (R) value is derived using the formula $P = V^2/R$, with a load assumed to be 2200 watts.

The fuel cell initially operates at 1 bar of pressure, allowing it to generate a maximum power of 2.6 kilowatts and power both the DC load and the battery. Excess fuel cell power is used to charge the battery. After 0.5 seconds, the fuel and air pressures are lowered to 0.001 bar, resulting in a drop in fuel cell power generation. During this period, the battery sends power to the load in order to maintain a power balance in the system, ensuring that the source and load power are always equal.

A step input block is used to simulate the change in fuel and air supply pressure. The step time is initially set to 0.5 seconds, keeping the pressure at 1 bar. The pressure changes to 0.001 bar after 0.5 seconds. Fuel cell power decreases as a result of this pressure change. Figure 5.5 and 5.4 show the fluctuations in battery voltage, current, power, and state of charge (SOC), as well as fuel

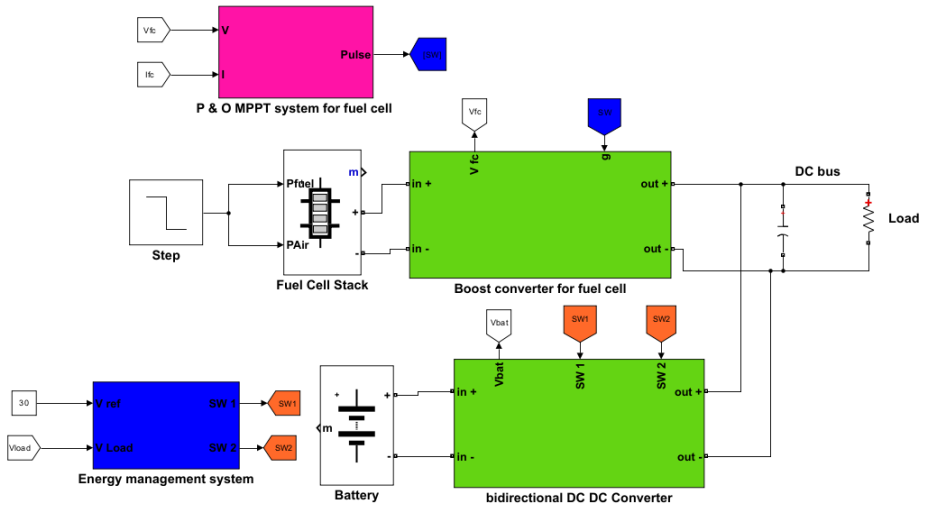

Figure 5.2: Simulated Diagram Of Fuel Cell Battery Hybrid System

cell voltage, current, and power. The response of the load voltage, current, and power can also be observed in Figure 5.6.

The fuel and air pressures are kept at 1 bar for the first 0 to 0.5 seconds. As represented in the figures, the fuel cell continues to operate at a voltage of 13 volts, a current of 200 amperes, and a power output of 2600 watts. The load voltage, load current, and load power remain at 30 volts, 73 amperes, and 2200 watts, respectively. According to this, the load only needs 2200 watts; however, the fuel cell produces 2600 watts, so the extra power can be used to charge the battery. The battery voltage is 15 volts, and the battery current is negative throughout this time, indicating that the battery is charging. The battery power is also negative, and the battery's SOC rises from 0 to 0.5 seconds, indicating that it is in charging mode.

The fuel and air pressures are reduced from 1 to 0.001 bar after 0.5 seconds. As a result, the fuel cell voltage and current drop to around 10 volts and 170 amperes, respectively, and the fuel cell produces around 1000 watts of power. Because of the reduced pressure, there is a power shortage in the load, and the battery begins supplying power to balance it. The numbers show that the battery current and power go from negative to positive, and the battery's SOC drops, suggesting that the battery is discharging. Despite the variation in fuel and air supply pressure, the load voltage, current, and power stay constant at 30 volts, 73 amps, and 2200 watts, respectively as shown in Figure 5.6. This illustrates that the load receives power from the sources constantly, thereby maintaining the power balance.

In summary, the simulation results of the fuel cell with battery energy storage system for a hybrid electric vehicle illustrate the system's dynamic behavior under various operating conditions. The fuel cell and battery work together to power the load, with any excess power used to charge the battery. The boost converter and bidirectional DC-DC converter control algorithms allow efficient power extraction from the fuel cell while maintaining a steady DC bus voltage. The system adjusts effectively to changes in fuel and air supply pressure, ensuring a balanced power flow to the load

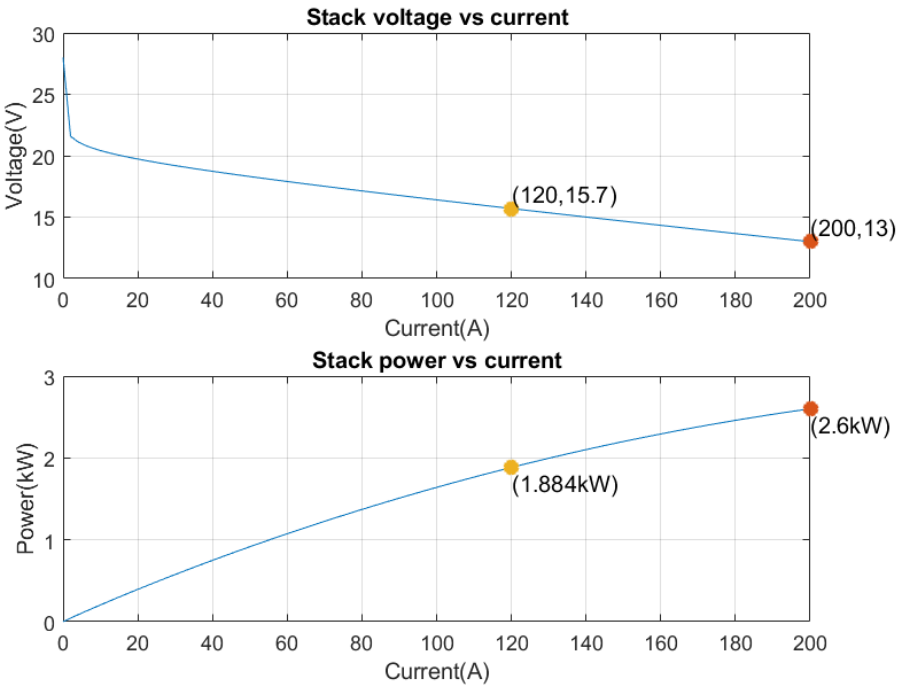

Figure 5.3: Fuel Cell Voltage and Power Curve

Table 5.1: Fuel Cell, Battery and Load Characteristic at variable Feul and Air Pressure

	Fuel Cell		battery		load	
Fuel and Air Pressure	1_{bar}	0.001_{bar}	1_{bar}	0.001_{bar}	1_{bar}	0.001_{bar}
$voltage(V)$	13 V	6 V	15 V	15 V	30 V	30 V
$current(I)$	200 A	170 A	- ve	73 A	73 A	73 A
$power(P)$	2600 W	1000 W	- ve	1200 W	2200 W	2200 W

and the hybrid electric vehicle's reliable operation. Table 5.1 shows the electric characteristic of the fuel cell, battery, and load at different fuel and air supply pressure. The parameters for the designed fuel cell and battery are attached in appendix D.

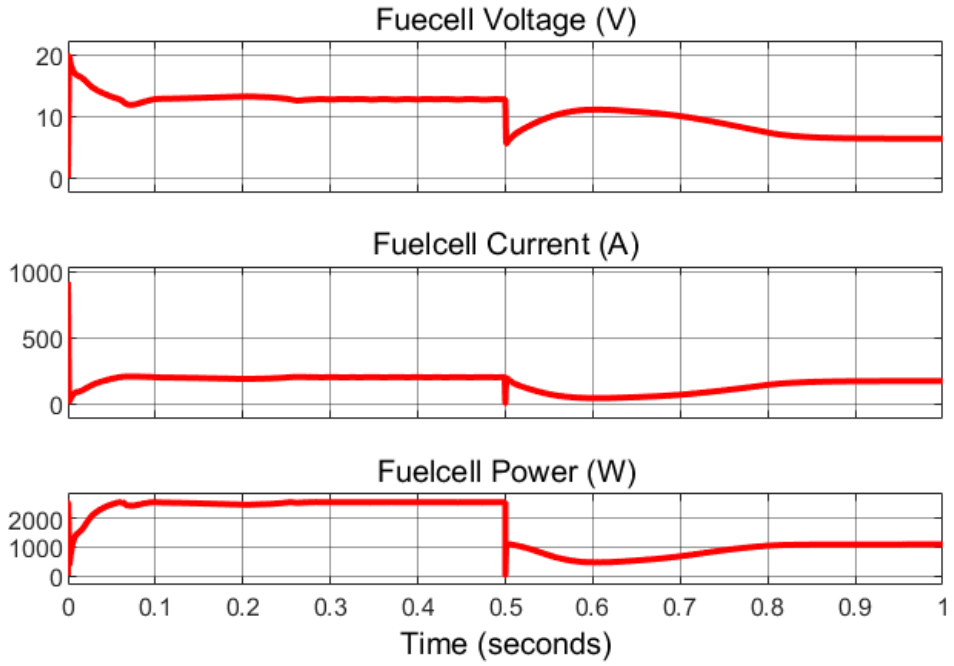

Figure 5.4: Fuel Cell Voltage Current and Power Curve During Step Decrease in Fuel and Air Pressure

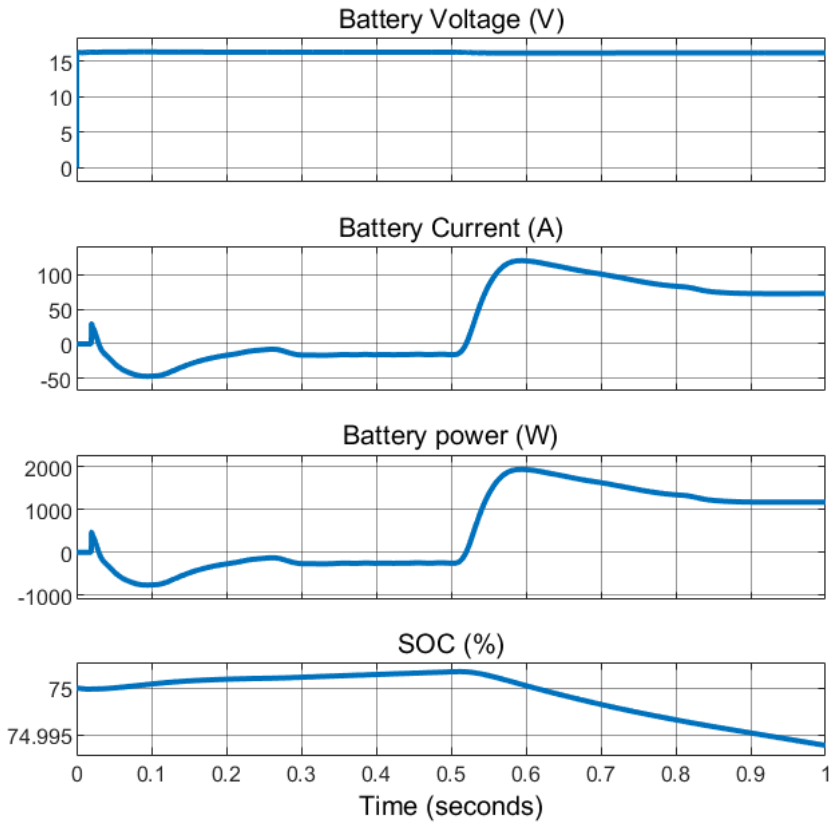

Figure 5.5: Battery Voltage, Current, Power, and SOC Curve

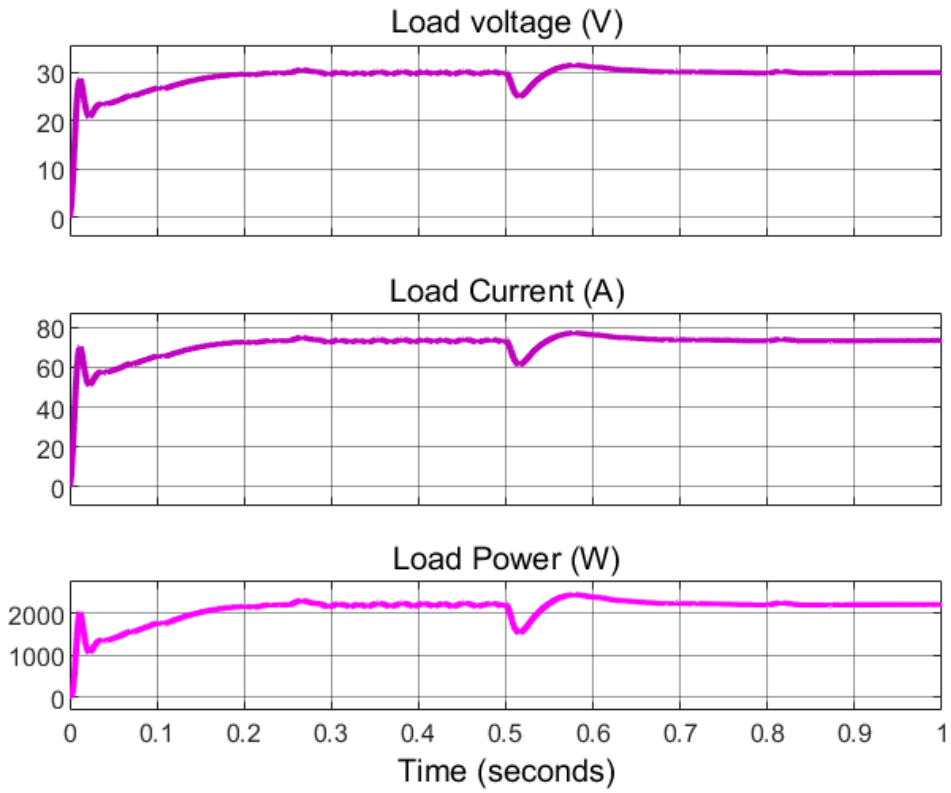

Figure 5.6: Load Voltage, Current and Power Curve

5.2 Fuel Cell, Battery, Supercapacitor Hybrid System Model

The circuit diagram shown in figure 5.7 shows the fuel cell battery supercapacitor hybrid system. The fuel cell side converter is the boost converter and it is unidirectional. The battery-side and the supercapacitor-side converter is the bidirectional converter (BDC) which allows the current to move in both directions. As the bidirectional converter is connected to the battery so during discharging of the battery the bidirectional converter will work in a boost mode. On the other hand, the bidirectional converter will work in buck mode when it is required to charge the battery.

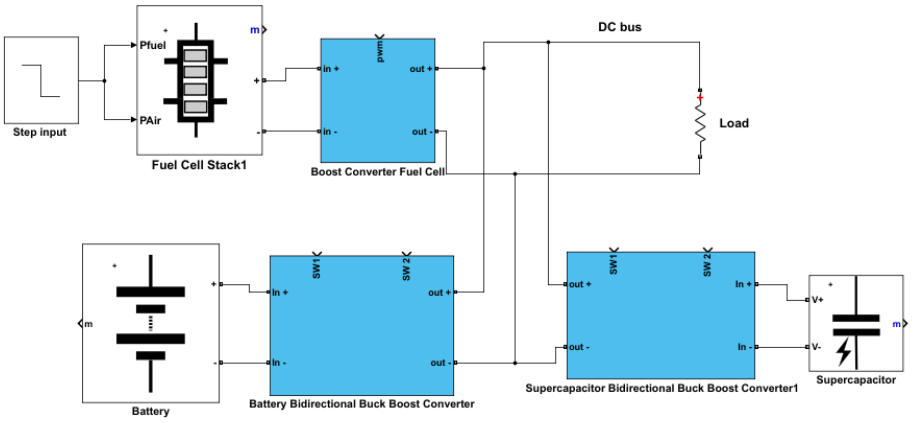

Figure 5.7: Simulated Diagram Of Fuel Cell, Battery, Supercapacitor Hybrid System

The simulation model for the fuel cell, battery, and, Supercapacitor, energy storage systems for hybrid electric vehicles is presented in Figure 5.7. In order to get the most power out of the fuel cell, the system comprises a fuel cell stack that is connected to a DC bus or DC load via a boost converter that is controlled by a maximum power point tracker ($MPPT$) P&0 controller. Optimizing energy management in the fuel cell, a battery-supercapacitor hybrid system using MATLAB Simulink with MPPT P&O (Perturb and Observe) optimization algorithm for both battery and supercapacitor is to develop and implement an advanced control strategy that maximizes the energy management between the battery and supercapacitor in an electric hybrid vehicle system. The DC bus is connected to the battery storage system and supercapacitor system, by a bidirectional $DC - DC$ converter, which includes the energy optimization algorithm as a control strategy for managing the energy flow between the battery and supercapacitor to keep the DC bus voltage constant around 30 volts.

In this model, the fuel cell and battery employed are similar to those used in the fuel cell battery hybrid system described in Section 5.1. However, a supercapacitor has been added as an energy storage system in order to assist in maintaining energy balance under variable load conditions. The model also utilizes the same maximum power point tracking ($MPPT$) and perturb and observe (P&O) algorithm as the fuel cell battery hybrid system. The main difference is that this model incorporates a control strategy that includes energy optimization algorithms to manage the energy flow between the battery and the supercapacitor. In summary, the model combines the familiar fuel cell and battery components with the addition of a supercapacitor and enhanced control strategy for improved energy management.

Performance evaluation

The system represented in Figure 5.7 was simulated using MATLAB/Simulink with *PI* controllers based on energy optimization techniques to evaluate the performance of the various design approaches of *PI* controllers. The following two operating conditions are taken into account:

- When Fuel and Air Pressure is 1 bar.
- When fuel and air pressure is 0.001 bar.

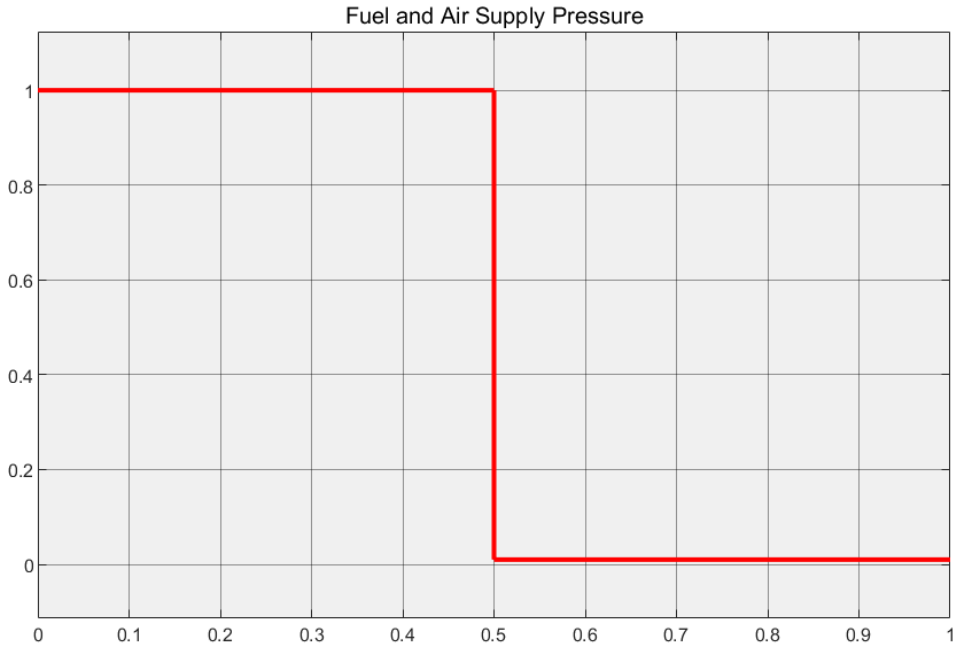

Figure 5.8: Step change in Fuel and Air pressure Curve

According to Figure 5.8, the fuel and air pressures utilized in this particular scenario are both set at 1 bar. In Figure 5.11, 5.12, the performance of the fuel cell, battery, and load under these conditions is presented. Initially, the load is solely powered by the fuel cell. From 0.5 to 1 second, when the fuel and air supply pressures drop to 0.01, the battery fully supports the load. In cases where the power requirement exceeds what the fuel cell can provide, the battery switches to discharge mode and supplies the additional power. Conversely, if there is excess power generated by the fuel cell, the battery switches to charge mode and stores the surplus energy.

Figure 5.10 illustrates the reactions of P_{sc} and P_{bat} to varying fuel and air pressures for fuel cells. These results demonstrate the usefulness of the HESS Battery Supercapacitor in conjunction with the designed PI controllers in improving the response of the Supercapacitor during storage or power release to reduce battery stress. For example, at 0.5 s, the power generated by the fuel cell decreases from around 2000 W to 800 W, and the battery shifts from discharging to charging mode. During this time, the excess electricity is stored in the Supercapacitor. The supercapacitor functions as a buffer during power shortages by providing rapid additional power, thereby minimizing the

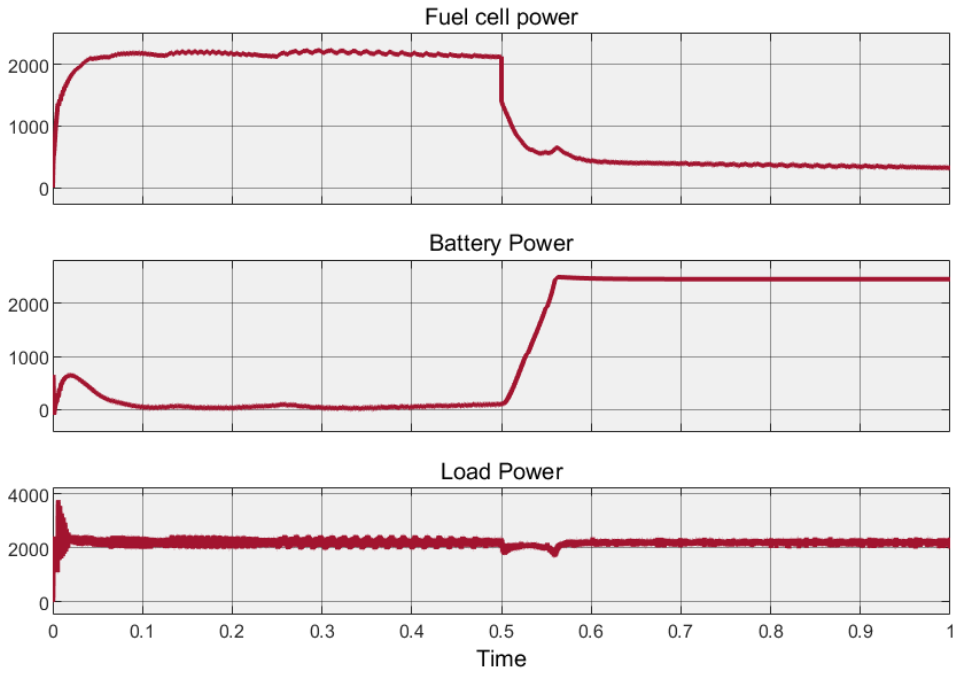

Figure 5.9: Responses of P_{FC}, P_{bat}, P_{Load} With Variable Fuel and Air Pressure

effects of load fluctuations on system stability.

The fuel cell in this system consistently generates a fixed power output of 2600 watts when the fuel and air supply pressures are set at 1 bar. In Figure 5.11, 5.12, the energy management strategy's effectiveness is depicted under varying fuel and air supply pressures. From 0 to 0.5 seconds, the load requires a power of 2200 watts, and during this period, the battery operates in charge mode, storing any excess power produced by the fuel cell. However, from 0.5 to 1 second, although the load power remains the same, the power supplied by the fuel cell decreases. In this time frame, the battery and supercapacitor operate in discharge mode to compensate for the insufficient power and supply the additional energy needed by the load.

The advantages of utilizing a Battery-Supercapacitor hybrid system can be clearly observed when PI controllers integrated with energy optimization techniques are employed. These control mechanisms enhance the performance of the Supercapacitor during the charging and discharging processes, leading to a significant reduction in the stress imposed on the battery. By optimizing the energy flow and distribution between the battery and Supercapacitor, the hybrid system can achieve improved response times and overall system efficiency.

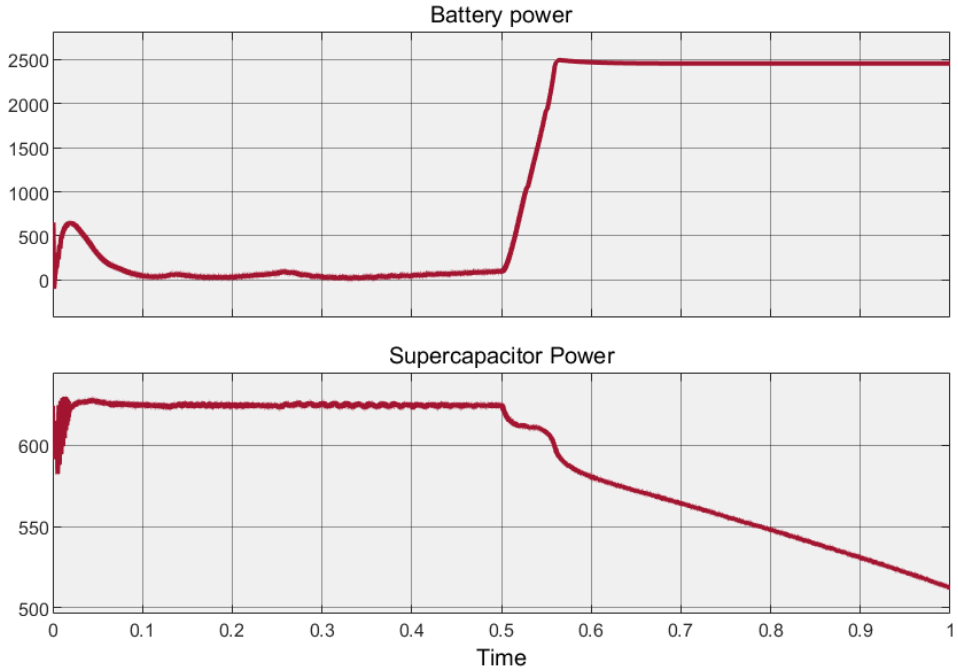

Figure 5.10: Responses of P_{SC}, P_{bat} With Variable Fuel and Air Pressure

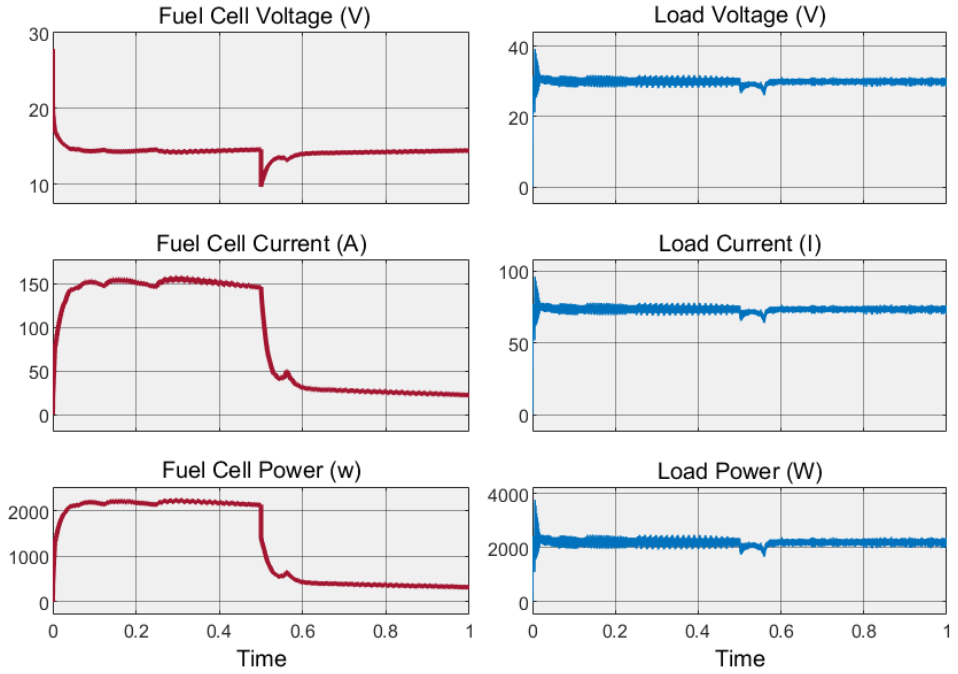

Figure 5.11: simulation curve of Fuel cell and Load under variable fuel and air pressure

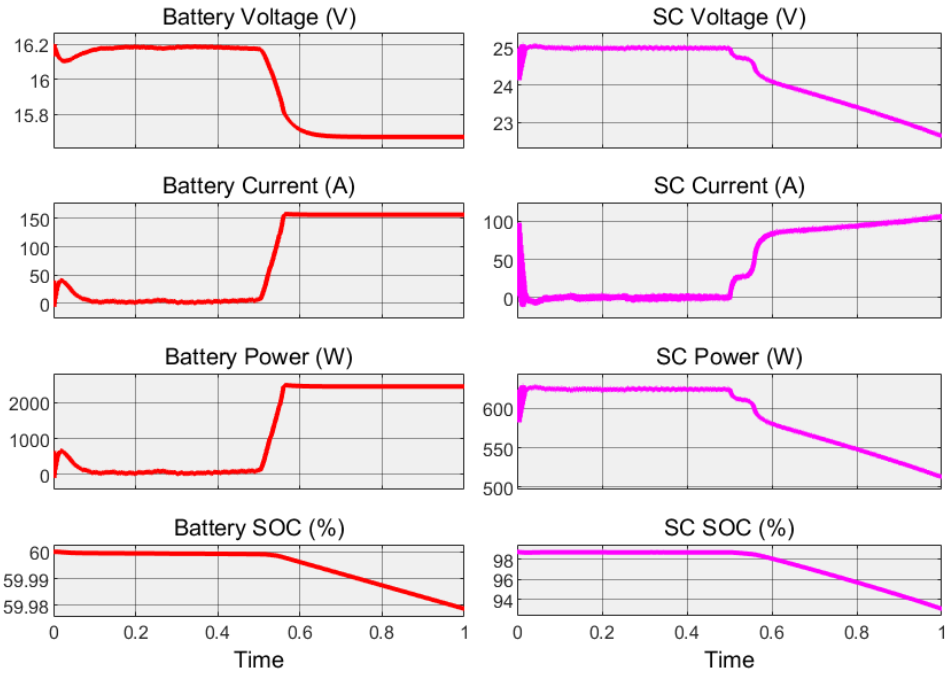

Figure 5.12: simulation curve of Battery and Supercapacitor Under Variable Fuel Air Supply Pressure

6

Discussion and Future Work

6.1 Discussion

- The objective of this research was to design and test a fuel cell stack and converter for a hybrid system in hydrogen fuel cell-based electric transport. The fuel cell stack and converter were developed using MATLAB Simulink (R2023a), and two phases of testing were conducted: one involving the fuel cell and battery, and the other incorporating the fuel cell, battery, and supercapacitor.

- The Simulation results demonstrated the successful implementation of the designed fuel cell stack and converter in the hybrid system. The performance and efficiency of the system were evaluated in terms of energy conversion and control utilizing MPPT P&O energy optimization technique. Overall, the system exhibited satisfactory energy conversion efficiency and met the desired objectives of providing power to the electric transport system i.e. the load power is equal to the source power.

- Comparing the obtained results with existing literature, it was observed that the designed fuel cell stack and converter performed reasonably well regarding energy conversion and control. The system showcased stable operation and demonstrated the potential for efficient power generation in hydrogen fuel cell-based electric transport.

- During the testing process, certain challenges were encountered, such as limitations in component availability and technical specifications available for fuel cells. However, These challenges had a minor impact on the design of the fuel cell system. furthermore, these limitations highlight the need for further improvements in the design and integration of the hybrid system.

Considerations

In this paper, the analysis of the driving cycle and different load changes was not considered, leaving room for future work to be conducted in those areas. However, the overall hybrid system was analyzed based on the variation of fuel and air supply pressure for the fuel cell. As discussed in earlier chapters, the fuel and air supply pressure was changed from 1 bar to 0.01 bar after 0.5 seconds, and the response of the system and load were analyzed accordingly.

For the fuel cell, it operates within a specific range to ensure optimum efficiency. When the fuel cell's power output matches the motor's requirements, the fuel cell becomes the sole power source for supplying the loads. However, if there is a disparity in the fuel and air pressure supply for the fuel cell, the battery and supercapacitor come into play to bridge the gap. These operational scenarios can be categorized into four modes, as presented below:

- Fuel Cell Only mode: When the fuel cell's power output meets the load requirements, the fuel cell acts as the primary power source, supplying the loads directly.

- Battery Discharge Mode: In cases where the fuel cell's power output is insufficient to meet the load demands, the battery enters discharge mode and supplies the additional power needed to bridge the gap.

- Battery Charge Mode: If the fuel cell's power output exceeds the load requirements, the excess power is used to charge the battery, ensuring efficient utilization of the fuel cell's energy generation.

- Supercapacitor Assistance Mode: The supercapacitor acts as a buffer during load fluctuations or sudden power demands, providing quick bursts of power to assist both the fuel cell and battery in meeting the load requirements.

These modes of operation allow for effective energy management and ensure a stable power supply to the loads while optimizing the overall efficiency of the hybrid system.

In future work, it is important to expand the analysis to include various driving cycles and load profiles to assess the performance of the hybrid system under different real-world scenarios. This would provide a more comprehensive evaluation of the system's capabilities and further optimize its operation for practical applications. Additionally, investigating control strategies and algorithms to dynamically adjust the power distribution among the fuel cell, battery, and supercapacitor based on real-time conditions could enhance the system's response, stability, and energy utilization.

6.2 Future Work

- To further enhance the performance of the hybrid system, future research should focus on optimizing the fuel cell stack design and converter control algorithms. Investigating advanced control strategies, such as model predictive control or fuzzy logic control, could improve the

system's response time, stability, and energy management capabilities.

- Exploring emerging technologies and components, such as advanced battery chemistries or high-performance supercapacitors, could also enhance the energy storage and delivery capabilities of the hybrid system. Integration of these components could lead to improved power density, extended range, and better overall system efficiency.

- Real-world validation and testing under various operating conditions are crucial to assess the system's performance and validate its potential for practical applications in hydrogen fuel cell-based electric transport. Future research should focus on conducting comprehensive field tests to evaluate the system's reliability, durability, and adaptability.

- Collaborations with other disciplines, such as material science or electrical engineering, could provide opportunities to explore novel materials for fuel cell stack construction, advanced power electronics for the converter design, or sophisticated control algorithms for optimized energy conversion and management.

Literature that can be taken into consideration for future work

In the field of vehicular systems, the management strategy of hybrid power source systems has gained significant attention, as evidenced by a wealth of academic literature. Several studies have addressed the challenge of meeting diverse load demands and optimizing system performance. The references below outline various control strategies and techniques used in this domain:

- Reference [[32]] presents an active power flow control algorithm that utilizes optimal control theory to meet different load demands efficiently.

- Thounthong et al. [[33]] propose an optimal control strategy aimed at minimizing fast transitions of energy devices to reduce stress on the system.

- Li et al. [[34]] introduce a strategy based on fuzzy logic control, which has been validated across different driving cycles.

- In reference [[35]], Li et al. present a power distribution strategy that combines wavelet transform and fuzzy logic control for efficient load management.

- Reference [[36]] proposes an optimal control strategy specifically designed for a city bus equipped with a proton exchange membrane (PEM) fuel cell.

- Sliding mode control for medium power fuel cell systems is explored in reference [[37]].

- In their work, Lopez et al. [[38]] implemented a rule-based power management system that incorporates a low pass filter to allocate power between the PEM fuel cell and the supercapacitors. The study focuses on analyzing the advantages of the energy management strategies employed, particularly in preventing oxygen starvation and reducing the frequency

of startups and shutdowns. By effectively distributing power between the fuel cell and supercapacitors, the proposed approach aims to optimize the overall performance and operational stability of the hybrid power system.

- Capasso et al. [[39]] develop an optimal control strategy for supercapacitors in a hybrid energy storage system. Their approach leverages the offline solution of an isoperimetric problem to dynamically optimize battery durability by reducing peak current.

- Zhang et al. [[40]] propose a novel configuration for fuel cell vehicles, utilizing strategic power management. In their system, three fuel cell stacks operate at fixed operating points, and the operation time is optimized through on-off switching control.

These references represent a sample of the extensive research conducted on the management strategies of hybrid power source systems. The mentioned studies employ various control techniques, including optimal control theory, fuzzy logic control, sliding mode control, model predictive control, and isoperimetric problem solutions. These approaches aim to improve load management, enhance system stability, reduce stress on energy devices, and optimize the overall efficiency of hybrid power systems in vehicular applications.

Future Research

The thesis has successfully designed a converter topology and implemented a control method for it. The feasibility of the design and control approach has been validated through simulations. However, to further enhance the system and address practical operational issues, future research aims to implement the designed converter and control approach on hardware. By testing the system on actual devices, valuable insights can be gained, enabling improvements based on real-world performance. Practical considerations, such as device integration, real-time response, and other operational challenges, will be taken into account during this phase. The hardware implementation and testing will provide valuable feedback for refining the design and control strategy, ultimately leading to an optimized and practical solution for the energy conversion and control of hydrogen fuel cell-based electric transport.

/7 Conclusion

To summarize, this paper introduces a generic model for analyzing the dynamic and steady-state characteristics of proton exchange membrane fuel cells (PEMFCs). The simulation results demonstrate the effectiveness of the fuel cell with battery energy storage system in a hybrid electric vehicle, showcasing its adaptability under various operating conditions. The integration of advanced control strategies, including maximum power point tracking (MPPT) algorithms and energy optimization techniques, ensures efficient power extraction and management. The fuel cell, battery, and supercapacitor work together to supply power to the load, with bidirectional converters facilitating power flow in both directions. The system demonstrates its ability to maintain a balanced power flow, even when fuel and air supply pressures vary. The battery and supercapacitor contribute to system stability and minimize stress on the battery, improving its longevity and overall performance.

In conclusion, the fuel cell battery supercapacitor hybrid system, supported by advanced control strategies, offers a promising solution for efficient energy management and enhanced performance in hybrid electric vehicles.

Bibliography

[1] O. Erdinc and M. Uzunoglu, *Recent trends in PEM fuel cell-powered hybrid systems: Investigation of application areas, design architectures and energy management approaches*. PhD thesis, 2010.

[2] S. Ahmadi, S. M. Bathaee, and A. H. Hosseinpour, "Improving fuel economy and performance of a fuel-cell hybrid electric vehicle (fuel-cell, battery, and ultra-capacitor) using optimized energy management strategy," *Energy Conversion and Management*, vol. 160, pp. 74–84, 3 2018.

[3] hussain I, *Husain, I. (2010). Electric and Hybrid Vehicles: Design Fundamentals, Second Edition (2nd ed.). CRC Press. https://doi.org/10.1201/9781439894972*.

[4] K. Song, F. Li, X. Hu, L. He, W. Niu, S. Lu, and T. Zhang, "Multi-mode energy management strategy for fuel cell electric vehicles based on driving pattern identification using learning vector quantization neural network algorithm," *Journal of Power Sources*, vol. 389, pp. 230–239, 6 2018.

[5] S. M. Haile, "Fuel cell materials and components," *Acta Materialia*, vol. 51, pp. 5981–6000, 11 2003.

[6] "Optimal Energy Management System for a Fuel Cell Hybrid Electric Vehicle Place for Project," tech. rep.

[7] energy education and https://energyeducation.ca/encyclopedia/Fuel_cell, "Fuel cell."

[8] R. E. Rosli, A. B. Sulong, W. R. Daud, M. A. Zulkifley, T. Husaini, M. I. Rosli, E. H. Majlan, and M. A. Haque, "A review of high-temperature proton exchange membrane fuel cell (HT-PEMFC) system," *International Journal of Hydrogen Energy*, vol. 42, pp. 9293–9314, 4 2017.

[9] F. De Bruijn and P. Veltman, "PEM fuel cells for telecom applications," in *INTELEC, International Telecommunications Energy Conference (Proceedings)*, 2011.

[10] A. G. Pukrushpan Jay T.
}and Stefanopoulou and P. Huei, "Background and Introduction," in *Control of Fuel Cell Power Systems: Principles, Modeling, Analysis and Feedback Design*, pp. 1–13, London: Springer London, 2004.

[11] M. J. Haubrock, D.-I. G. Heideck, and Z. Styczynski, "Electrical efficiency losses occurred by

the air compressor for PEMFC," tech. rep.

[12] J. Larminie and A. Dicks, *Fuel cell systems explained*. J. Wiley, 2003.

[13] A. Akroot, Ekici, and M. Köksal, "Process modeling of an automotive pem fuel cell system," *International Journal of Green Energy*, vol. 16, pp. 778–788, 8 2019.

[14] H. S. Das, C. W. Tan, and A. H. Yatim, "Fuel cell hybrid electric vehicles: A review on power conditioning units and topologies," *Renewable and Sustainable Energy Reviews*, vol. 76, pp. 268–291, 9 2017.

[15] B. Nykvist and O. Olsson, "The feasibility of heavy battery electric trucks," *Joule*, vol. 5, pp. 901–913, 4 2021.

[16] V. Mounica and Y. P. Obulesu, "Hybrid Power Management Strategy with Fuel Cell, Battery, and Supercapacitor for Fuel Economy in Hybrid Electric Vehicle Application," *Energies*, vol. 15, 6 2022.

[17] K. Mammar and A. Chaker, "Neural Network-Based Modeling of PEM fuel cell and Controller Synthesis of a stand-alone system for residential application," tech. rep., 2012.

[18] X. Huang, Z. Zhang, and J. Jiang, "Fuel cell technology for distributed generation: An overview," in *IEEE International Symposium on Industrial Electronics*, vol. 2, pp. 1613–1618, 2006.

[19] "UNIVERSITÀ DEGLI STUDI DI TRIESTE XVII CICLO DEL DOTTORATO DI RICERCA IN SCIENZE DELL'INGEGNERIA-INDIRIZZO INGEGNERIA MECCANICA, NAVALE, DELL'ENERGIA E DELLA PRODUZIONE Electrocatalyst degradation in high temperature PEM fuel cells," tech. rep.

[20] S. A. Ansari and J. S. Moghani, "A Novel High Voltage Gain Noncoupled Inductor SEPIC Converter," *IEEE Transactions on Industrial Electronics*, vol. 66, pp. 7099–7108, 9 2019.

[21] J. Rekha, T. M. Thamizh Thentral, and K. Vijayakumar, "Electric Vehicle Motor, Converter, Controller and Charging Station with Challenges and Configurations: Review," Tech. Rep. 1, 2022.

[22] S. Ranjan Behera and T. Kumar Meher, "DESIGN OF SINGLE ENDED PRIMARY INDUCTOR DC-DC CONVERTER," tech. rep.

[23] S. K. George, E. Paul, E. P. Babu, S. Mathew, and G. James, "A High Gain Bidirectional SEPIC Converter," *International Journal of Engineering Research and Applications www.ijera.com*, vol. 11, pp. 36–43, 2021.

[24] S. M. Chen, M. L. Lao, Y. H. Hsieh, T. J. Liang, and K. H. Chen, "A novel switched-coupled-inductor DC-DC step-Up converter and its derivatives," *IEEE Transactions on Industry Applications*, vol. 51, pp. 309–314, 1 2015.

[25] R. Gules, W. M. Dos Santos, R. C. Annunziato, E. F. R. Romaneli, and C. Q. Andrea, "A modified SEPIC converter with high static gain for renewable applications," in *COBEP 2011 - 11th Brazilian Power Electronics Conference*, pp. 162–167, 2011.

[26] M. A. Salvador, T. B. Lazzarin, and R. F. Coelho, "High Step-Up DC-DC Converter with Active Switched-Inductor and Passive Switched-Capacitor Networks," *IEEE Transactions on Industrial Electronics*, vol. 65, pp. 5644–5654, 7 2018.

[27] S. Pattabiraman, "Wind Energy Based Mobile Battery Charging and Battery Applications Thermal Sensor for Flow Measurements View project Tracking Solutions in IoT-LPWAN View project Methods Enriching Power and Energy Development (MEPED) 2014 Wind Energy Based Mobile Battery Charging and Battery Applications," tech. rep., 2014.

[28] D. Feroldi, M. Serra, and J. Riera, "Design and analysis of fuel-cell hybrid systems oriented to automotive applications," *IEEE Transactions on Vehicular Technology*, vol. 58, pp. 4720–4729, 11 2009.

[29] L. Fan and X. Ma, "Maximum power point tracking of PEMFC based on hybrid artificial bee colony algorithm with fuzzy control," *Scientific Reports*, vol. 12, 12 2022.

[30] M. YILMAZ and M. CORAPSİZ, "Artificial Neural Network based MPPT Algorithm with Boost Converter topology for Stand-Alone PV System," *Erzincan Üniversitesi Fen Bilimleri Enstitüsü Dergisi*, vol. 15, pp. 242–257, 3 2022.

[31] A. Lukman Setya Budi, S. Anam, M. Ashari, and A. Soeprijanto, "Energy Management Control Based on Standalone Photovoltaic Battery and Supercapacitor Hybrid Energy Storage System Using PI Controller," tech. rep., 2020.

[32] Z. Yu, D. Zinger, and A. Bose, "An innovative optimal power allocation strategy for fuel cell, battery and supercapacitor hybrid electric vehicle," *Journal of Power Sources*, vol. 196, pp. 2351–2359, 2 2011.

[33] P. Thounthong, S. Raël, and B. Davat, "Energy management of fuel cell/battery/supercapacitor hybrid power source for vehicle applications," *Journal of Power Sources*, vol. 193, pp. 376–385, 8 2009.

[34] Q. Li, W. Chen, Y. Li, S. Liu, and J. Huang, "Energy management strategy for fuel cell/battery/ultracapacitor hybrid vehicle based on fuzzy logic," *International Journal of Electrical Power and Energy Systems*, vol. 43, pp. 514–525, 12 2012.

[35] Q. Li, W. Chen, Z. Liu, M. Li, and L. Ma, "Development of energy management system based on a power sharing strategy for a fuel cell-battery-supercapacitor hybrid tramway," *Journal of Power Sources*, vol. 279, pp. 267–280, 4 2015.

[36] L. Xu, M. Ouyang, J. Li, F. Yang, L. Lu, and J. Hua, "Application of Pontryagin's Minimal Principle to the energy management strategy of plugin fuel cell electric vehicles," *International Journal*

of Hydrogen Energy, vol. 38, pp. 10104–10115, 8 2013.

[37] F. Segura and J. M. Andújar, "Power management based on sliding control applied to fuel cell systems: A further step towards the hybrid control concept," *Applied Energy*, vol. 99, pp. 213–225, 2012.

[38] G. Lopez Lopez, R. Schacht Rodriguez, V. M. Alvarado, J. F. Gomez-Aguilar, J. E. Mota, and C. Sandoval, "Hybrid PEMFC-supercapacitor system: Modeling and energy management in energetic macroscopic representation," *Applied Energy*, vol. 205, pp. 1478–1494, 11 2017.

[39] C. Capasso, D. Lauria, and O. Veneri, "Optimal control strategy of ultra-capacitors in hybrid energy storage system for electric vehicles," in *Energy Procedia*, vol. 142, pp. 1914–1919, Elsevier Ltd, 2017.

[40] H. Zhang, X. Li, X. Liu, and J. Yan, "Enhancing fuel cell durability for fuel cell plug-in hybrid electric vehicles through strategic power management," *Applied Energy*, vol. 241, pp. 483–490, 5 2019.

A

Simulation of The Fuel Cell, Battery, and Supercapacitor Used For Hybrid Electric Vehicle .

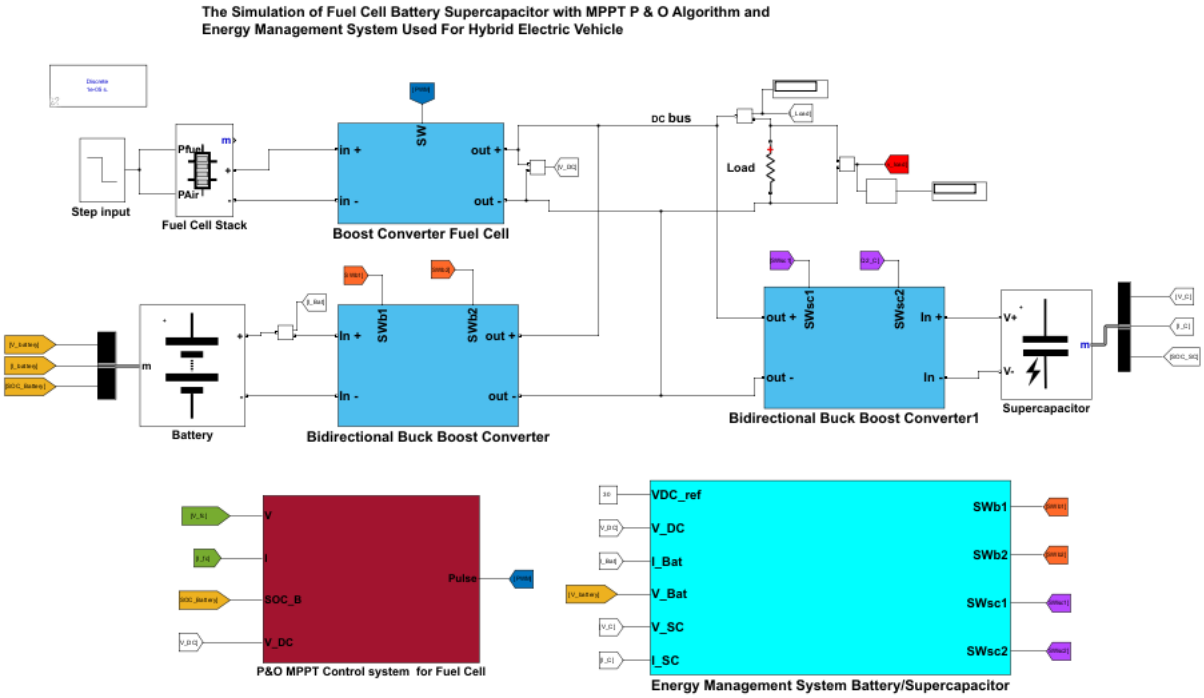

The Simulation of MPPT P & O Algorithm With Energy Optimization Technique

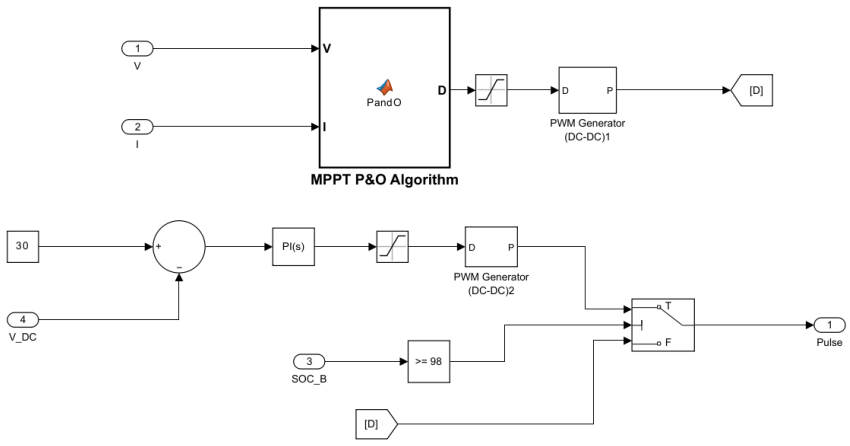

The Simulation Boost Converter Used for Fuel Cell

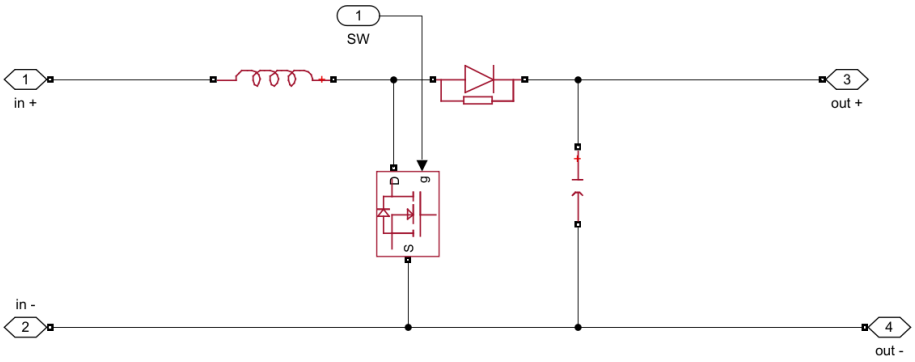

The Simulation of Energy Management System Battery and SuperCapacitor

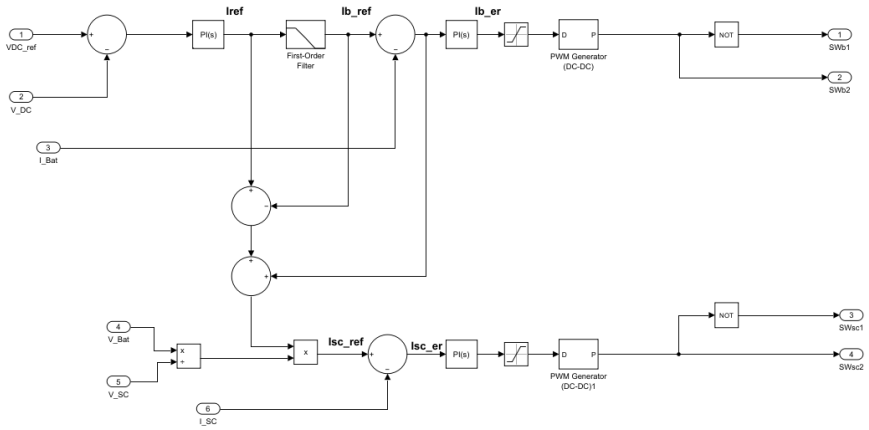

The Simulation of Bidirectional Converter

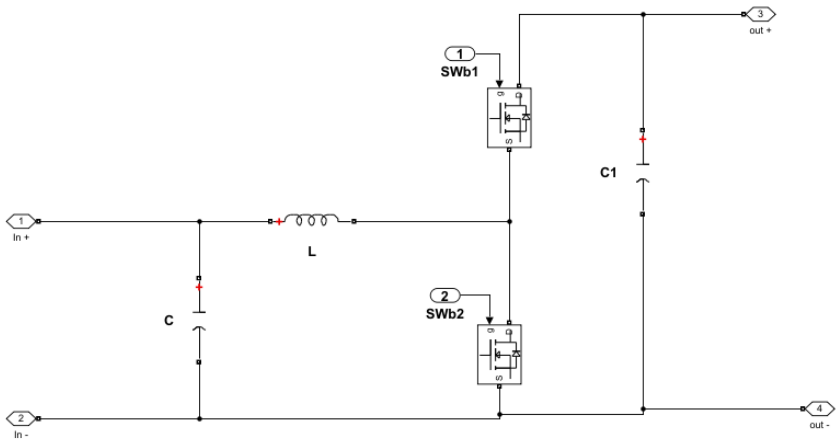

B

MATLAB Block Diagram Designed in Simulink

B.0.1 MATLAB Block Diagram

Simulation of the PEM fuel cell under Various losses

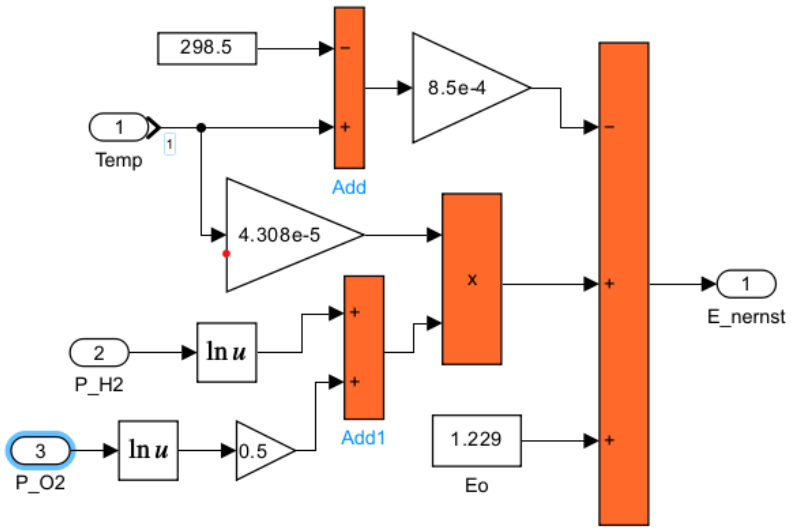

[htbp]

Figure B.1: E Nernst Simulation Block Diagram Model.

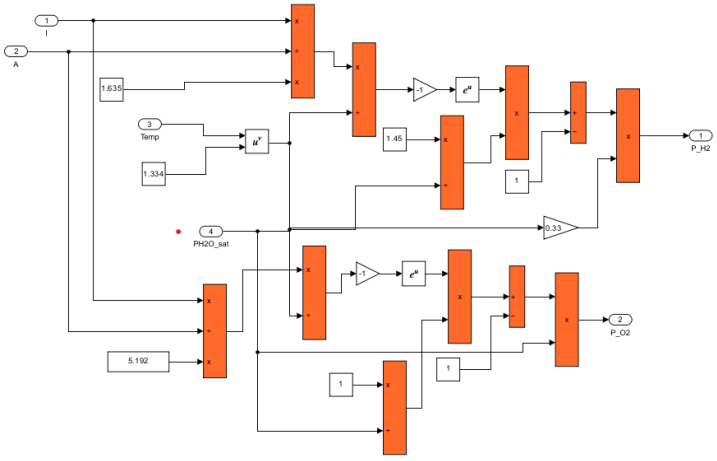

[htbp]

Figure B.2: Oxygen and Hydrogen Partial Pressure Model.

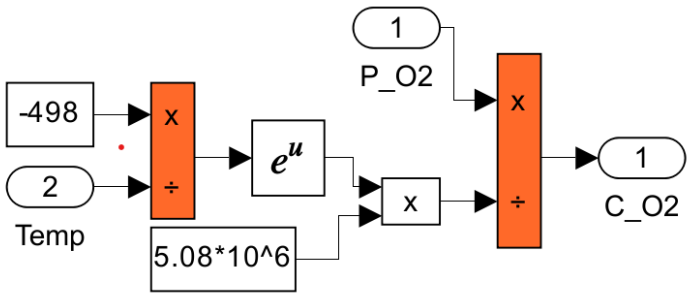

[htbp]

Figure B.3: Oxygen Concentration Block Diagram Model.

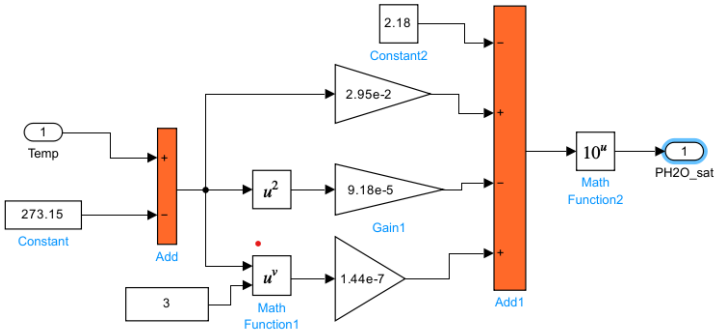

[htbp]

Figure B.4: Saturation Pressure of H_2 Model.

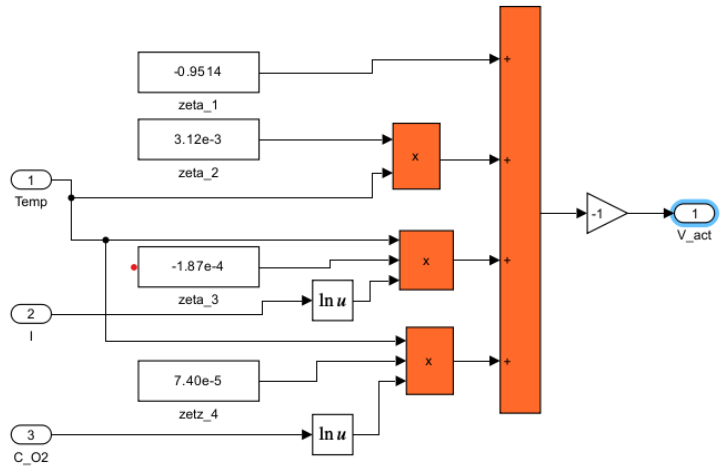

[htbp]

Figure B.5: Activation Losses Block Diagram Model.

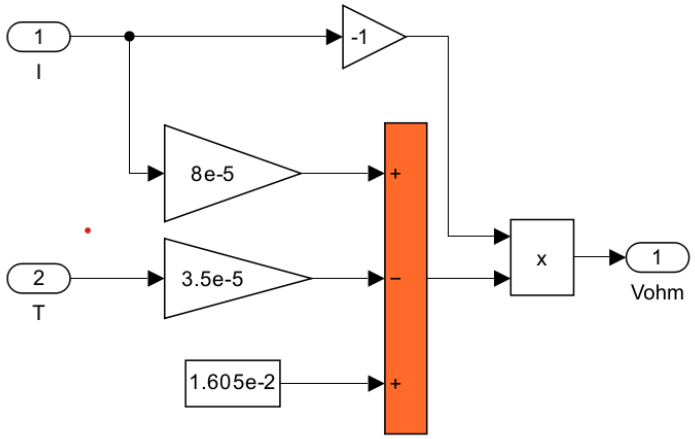

[htbp]

Figure B.6: Ohmic Losses Block Diagram Model.

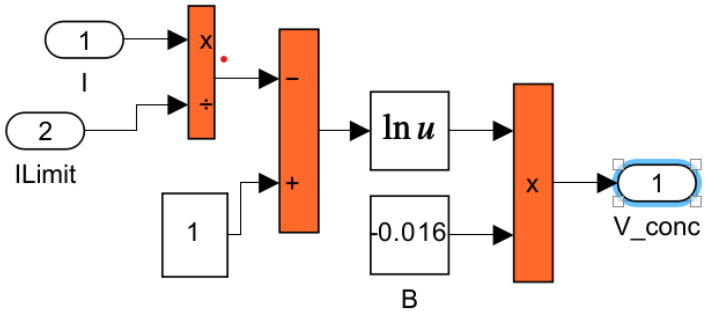

[htbp]

Figure B.7: Concentration Losses Block Diagram Model.

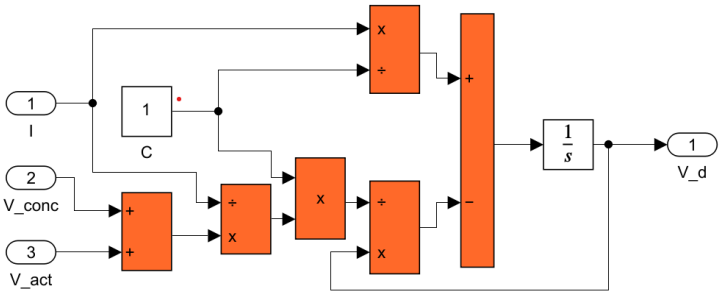

[htbp]

Figure B.8: Dynamic Losses Block Diagram Model.

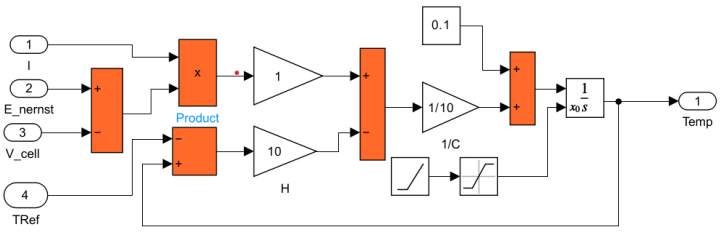

[htbp]

Figure B.9: Thermodynamic Losses Block Diagram Model.

C

MATLAB Code For Designing The Fuel Cell Stack.

C.1 Design of Fuel Cell in MATLAB Script

```
% Your MATLAB code here

%function V_out  = fcn(ifc,Tc,P_H2,P_air)

%design of fuel cell in matlab script

% Input parameters

P_H2=3;  % Hydrogen pressure in atm
P_air=3;   % Air pressure in atm
A_cell=100.8;   %Area of cell
N_cells=14;  % Number of cells
r=0.19;  % Internal Resistance (Ohm-cm^2)
R=8.314;   % ideal gas constant(J/molK)
F=96487;   % Faradays constant (Columbs)
Tc=45;  %Temperature in degree C
K=1.1;   % Constant k used in mass transport
io=10^-6.912;   % Exchange Current Density (A/cm^2)
iL=1.4;  % Limitimg Current Density (A/cm^2)
Gf_liq=-228170;   % Gibbs function in liquid form (J/mol)
Alpha =0.5;  % Transfer Coefficient
Alpha1=0.085;   %Amplification constant

%%%%%%%%%%%%%%%%%%%%%%%%%%%%%%%%%%%%%%%%%%%%%%%%%%%%%%%%%%%%%%%%%%%%%%%%%%%%%%%

%convert Degree Celcius to Kelvin
Tk=Tc+273.15;
```

```
28
29 % Create loop for current
30
31 Loop=1;
32 ifc=0;
33 for N=0:150
34     ifc=ifc+0.01;
35
36 % Calculation of partial pressures
37
38 % Calculation of saturation pressure of water
39 x=-2.1794 + 0.02953*Tc-9.1837*(10^-5)*(Tc^2) + 1.4454*(10^-7)*(Tc^3);
40 P_H2O=(10^x);
41
42 % Calculation of partial pressure of hydrogen
43
44 %PP_H2=0.5*((P_H2)/(exp(1.653*ifc/(Tk^1.334)))-P_H2O);
45 PP_H2=0.5*((P_H2)/(exp(1.653*ifc/(Tk^1.334)))-P_H2O);
46
47 % calculation of partial pressure of oxygen
48
49 PP_O2=(P_air/exp(4.192*ifc/(Tk^1.334)))-P_H2O;
50
51
52 %%%%%%%%%%%%%%%%%%%%%%%%%%%%%%%%%%%%%%%%%%%%%%%%%%%%%%%%%%%%%%%%%%%%%%%
53 % Activation Loss
54
55 b=R.*Tk./(2.*Alpha.*F);
56 V_act=-b.*log10(ifc./io);  % Tafel equation
57 %z1=-0.9514;
58 %z2=0.00312;
59 %z3=7.4*10^-5;
60 %z4=-1.87*10^-5;
61
62 %Co2=P_air/5.08*10^6*exp(-498/Tk);
63
64 %V_act=-(z1+z2*Tk+z3*Tk*(log(Co2))+z4*Tk*(log(ifc)));
65 % Ohmic Losses
66
67 V_ohmic=-(ifc*r);
68
69 %Mass Transport Losses
70
71 term = (1-(ifc./iL));
72 if term>0
73     V_conc=Alpha1*(ifc^K)*log(1-(ifc/iL));
74 else
75     V_conc=0;
76 end
77
78 % Calculation of Nernst Voltage
79
80 E_nernst= -Gf_liq/(2*F) - ((R*Tk)*log(P_H2O/(PP_H2*(PP_O2^0.5))))/(2*F);
81
82 %Calculation of Output Voltage
83
84 V_out = E_nernst +V_ohmic+V_act+V_conc;
```

```
if term<0
    V_conc=0;
    break
end
if V_out<0
    V_out=0;
    break
end

figure(1);
title('Fuel Cell Polarization Curve');
xlabel('Current density (A/cm^2)');
ylabel('Output Voltage(Volts)');
plot(ifc, V_out,"*");
grid on;
hold on;
disp(V_out);

% Calculation of power

P_out=N_cells.*V_out.*ifc.*A_cell;
figure(2);
title('Fuel Cell Power');
xlabel('Current density (A/cm^2)');
ylabel('Power(watts)');
plot(ifc, P_out, '*');
grid on;
hold on;
disp(P_out);


figure(3);
title('activation loss');
xlabel('Current density (A/cm^2)');
ylabel('activation loss)');
plot(ifc, V_act, '*');
grid on;
hold on;
disp(P_out);

figure(4);
title('ohmic loss');
xlabel('Current density (A/cm^2)');
ylabel('ohmic loss)');
plot(ifc, V_ohmic, '*');
grid on;
hold on;
disp(P_out);

figure(5);
title('concentration loss');
xlabel('Current density (A/cm^2)');
ylabel('concentration loss');
plot(ifc, V_conc, '*');
grid on;
hold on;
disp(P_out);
```

```
142
143 figure(6);
144 title('nernst voltage');
145 xlabel('Current density (A/cm^2)');
146 ylabel('nernst voltage');
147 plot(ifc, E_nernst, '*');
148 grid on;
149 hold on;
150 disp(P_out);
151 end
```

Listing C.1: MATLAB Script

C.2 The output From The MATLAB code.

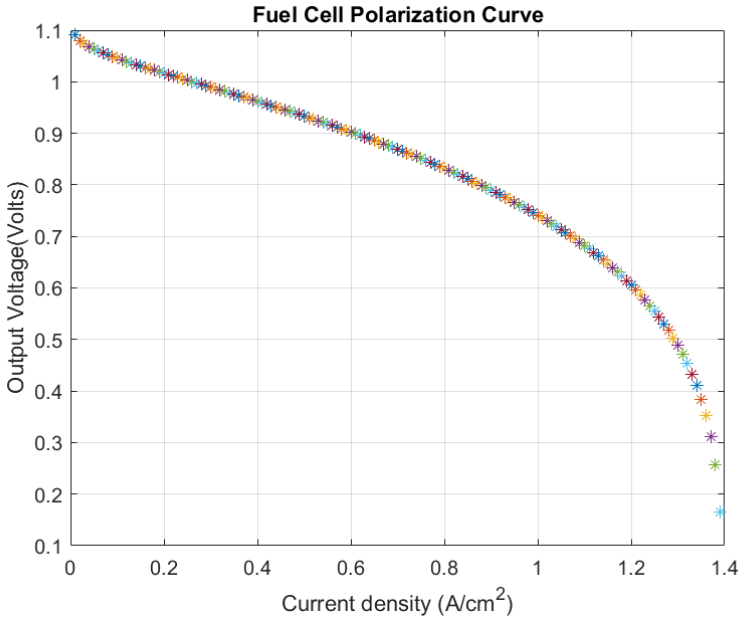

Figure C.1: Polarization Curve.

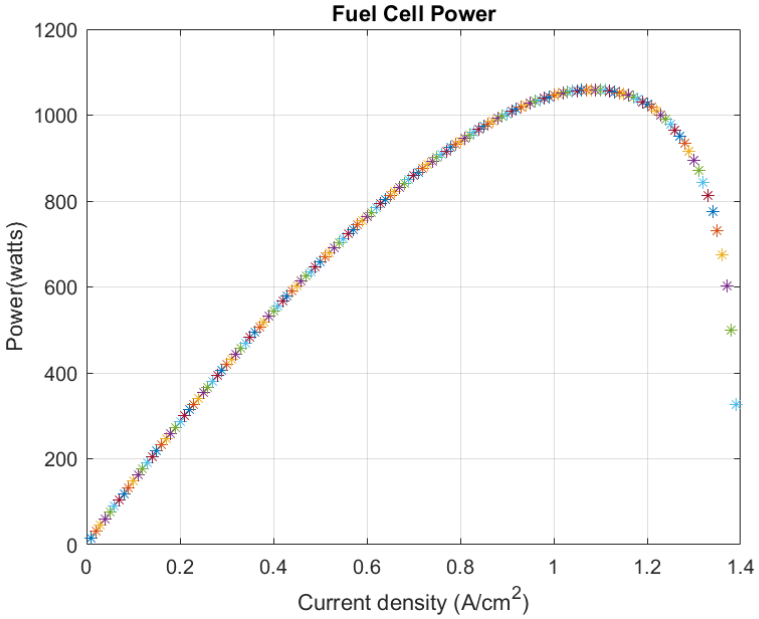

Figure C.2: Power Of Fuel Cell Stack.

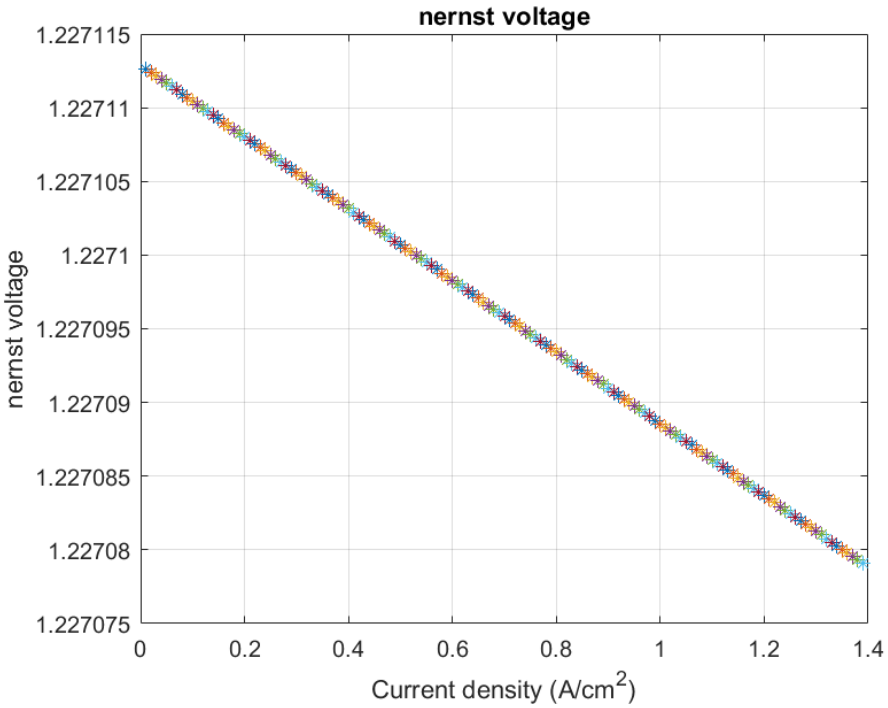

Figure C.3: Nernst Potential.

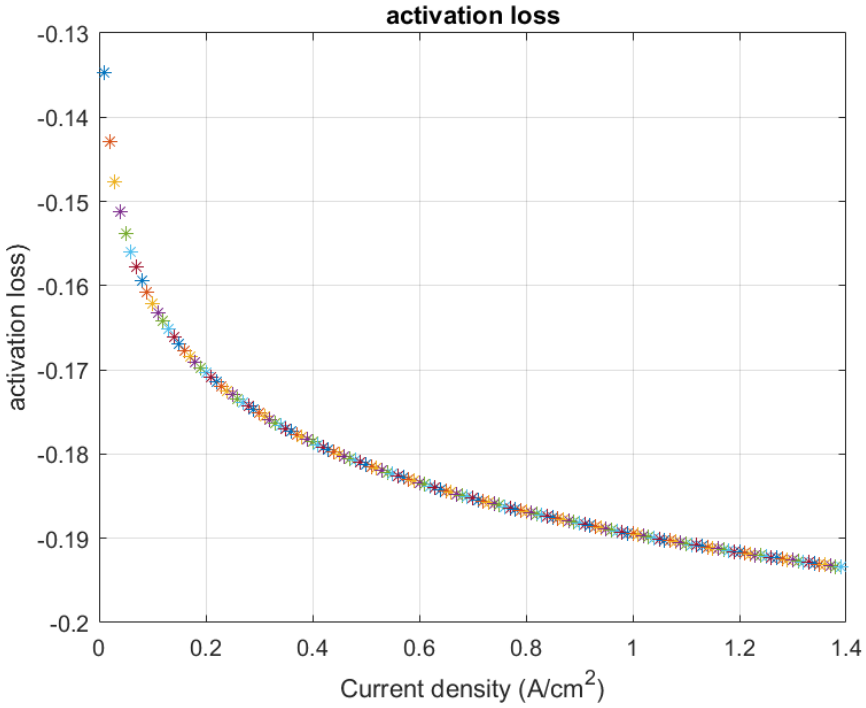

Figure C.4: Activation Losses.

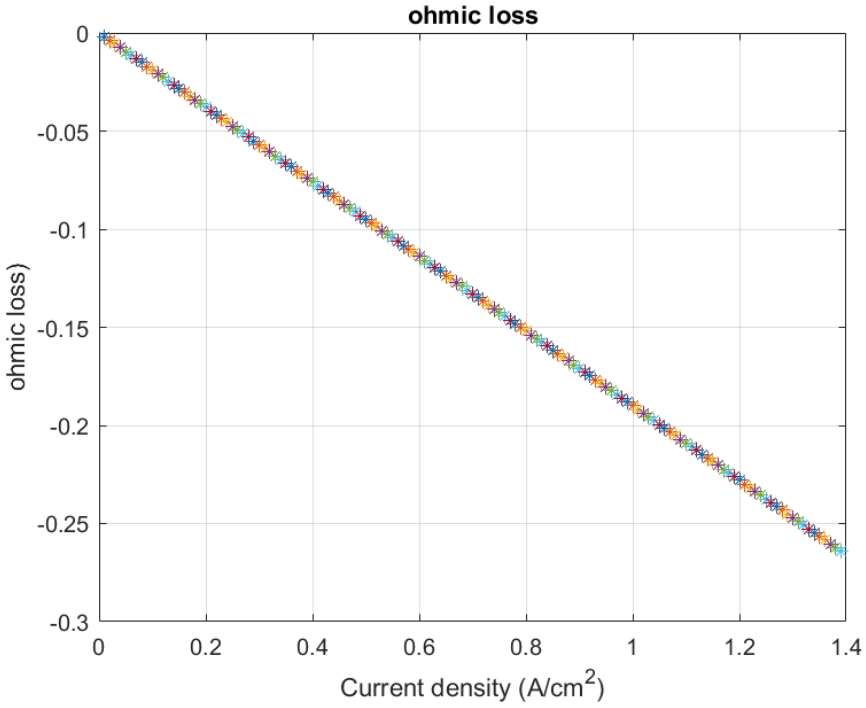

Figure C.5: Ohmic Losses.

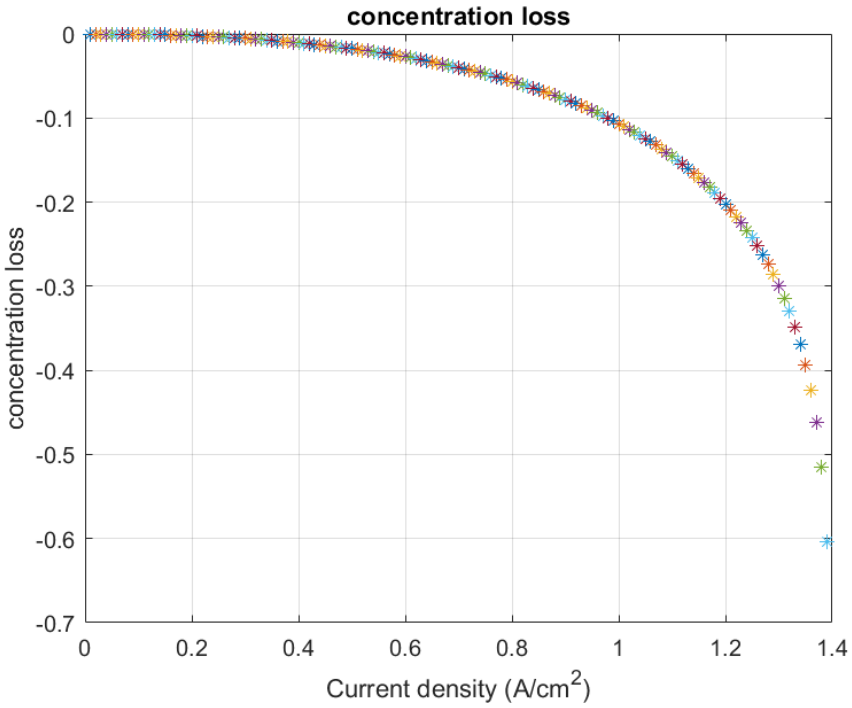

Figure C.6: Concentration Losses.

Parameters For The Fuel Cell and Battery For Fuel Cell Battery Hybrid System

D.1 Fuel Cell Parameters

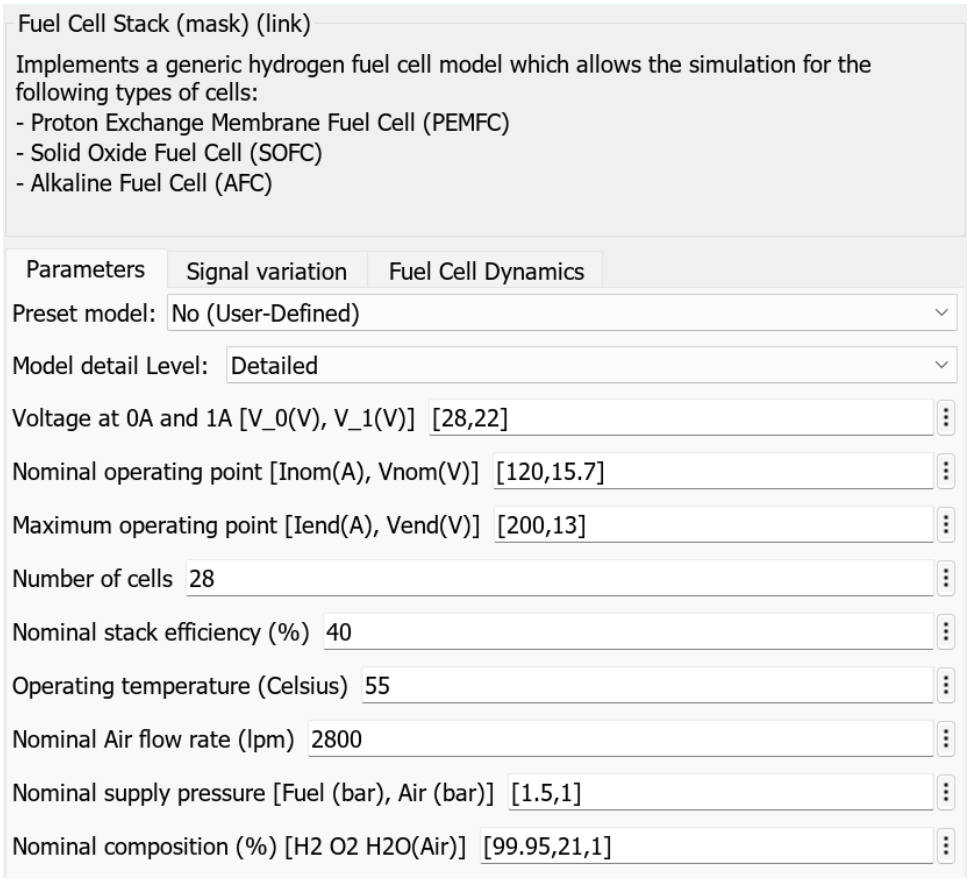

Figure D.1: Used Parameter For Fuel Cell.

```
Fuel cell nominal parameters:
  Stack Power:
      -Nominal = 1884 W
      -Maximal = 2600 W
  Fuel Cell Resistance = 0.030129 ohms
  Nerst voltage of one cell [En] = 1.1849 V
  Nominal Utilization:
      -Hydrogen (H2)= 89.4 %
      -Oxidant  (O2)= 2.391 %
  Nominal Consumption:
      -Fuel = 23.42 slpm
      -Air  = 55.72 slpm
  Exchange current [i0] = 2.6763e-05 A
  Exchange coefficient [alpha] = 0.69788

Fuel cell signal variation parameters:
  Fuel composition [x_H2] = 99.95 %
  Oxidant composition [y_O2] = 21 %
  Fuel flow rate [FuelFr] at nominal Hydrogen utilization:
      -Nominal = 20.98 lpm
      -Maximum = 34.96 lpm
  Air flow rate [AirFr] at nominal Oxidant utilization:
      -Nominal = 2800 lpm
      -Maximum = 4667 lpm
  System Temperature [T] = 328 Kelvin
  Fuel supply pressure [Pfuel] = 1.5 bar
  Air supply pressure [PAir] = 1 bar
```

Figure D.2: Parameters Foe Fuel Cell.

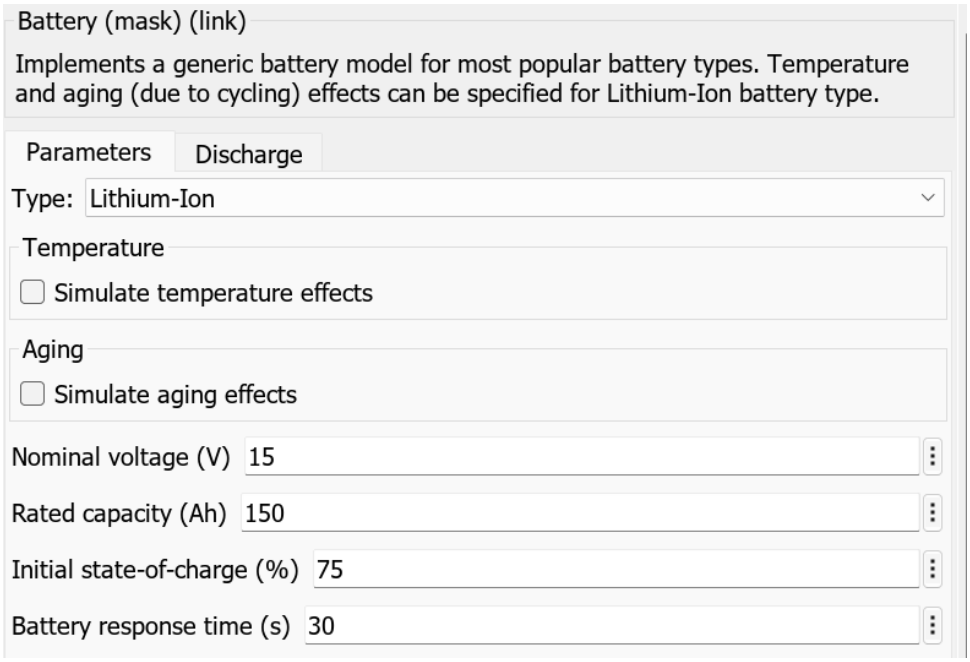

Figure D.3: Battery parameters.